Osteological Redescription of the Late Triassic Sauropodomorph Dinosaur Thecodontosaurus antiquus Based on New Material from Tytherington, Southwestern England

Authors: Ballell, Antonio, Rayfield, Emily J., and Benton, Michael J.

Source: Journal of Vertebrate Paleontology, 40(2)

Published By: The Society of Vertebrate Paleontology

URL: https://doi.org/10.1080/02724634.2020.1770774

Journal of Vertebrate Paleontology e1770774 (24 pages)

DOI: 10.1080/02724634.2020.1770774

ARTICLE

OSTEOLOGICAL REDESCRIPTION OF THE LATE TRIASSIC SAUROPODOMORPH DINOSAUR *THECODONTOSAURUS ANTIQUUS* BASED ON NEW MATERIAL FROM TYTHERINGTON, SOUTHWESTERN ENGLAND

ANTONIO BALLELL, * EMILY J. RAYFIELD, and MICHAEL J. BENTON
School of Earth Sciences, University of Bristol, Bristol, BS8 1RJ, United Kingdom, ab17506@bristol.ac.uk; e.rayfield@bristol.ac.uk; mike.benton@bristol.ac.uk

ABSTRACT—*Thecodontosaurus antiquus* is a basal sauropodomorph from the Rhaetian locality of Durdham Down in Bristol, U.K. Sauropodomorph material putatively assigned to this species was found at the nearby site of Tytherington. Here, we describe the Tytherington specimens and compare them with *T. antiquus* and other Late Triassic sauropodomorphs from Britain. We find that this material can be assigned to *T. antiquus* based on multiple shared morphological traits, and we provide a revised diagnosis of this taxon. The new anatomical information from the Tytherington specimens enriches the osteology of the species, particularly of previously unknown parts of the skeleton such as the skull. We find poor anatomical support to distinguish the contemporary *Pantydraco caducus* from *T. antiquus*, such that the former might represent a juvenile of the latter. We also discuss the questionable validity of *Asylosaurus yalensis*. *Thecodontosaurus antiquus* is one of the most basal sauropodomorphs that show craniodental traits related to herbivory, while retaining a plesiomorphic limb morphology and posture. This taxon was an important component of Rhaetian insular ecosystems of southwestern Britain.

SUPPLEMENTAL DATA—Supplemental materials are available for this article for free at www.tandfonline.com/UJVP

Citation for this article: Ballell, A., E. J. Rayfield, and M. J. Benton. 2020. Osteological redescription of the Late Triassic sauropodomorph dinosaur *Thecodontosaurus antiquus* based on new material from Tytherington, southwestern England. Journal of Vertebrate Paleontology. DOI: 10.1080/02724634.2020.1770774.

INTRODUCTION

Dinosaurs are a clade of avemetatarsalian archosaurs that originated in Gondwana in the Middle–Late Triassic (Marsola et al., 2019), splitting early in their history into three main lineages (Baron et al., 2017; Langer et al., 2017) and rising to ecological dominance by the Early Jurassic (Brusatte et al., 2008a, 2008b). One of these lineages, Sauropodomorpha, rapidly radiated to give rise to a diverse assemblage of Carnian taxa in southern Gondwana (Langer et al., 1999; Martínez and Alcober, 2009; Ezcurra, 2010; Cabreira et al., 2011, 2016; Sereno et al., 2013). After this early diversification, sauropodomorphs, as well as other dinosaurs, migrated also to northern latitudes, and by the Norian and Rhaetian, Laurasia was inhabited by several early members of this clade of dinosaurs (Marsola et al., 2019). One of these Late Triassic sauropodomorphs was *Thecodontosaurus antiquus*, which lived in the region that today forms the British Isles (Benton et al., 2000) and occupies a basal phylogenetic position as a non-plateosaurian (sensu Yates, 2007) sauropodomorph (Benton et al., 2000; Otero and Pol, 2013; Langer et al., 2019).

Thecodontosaurus was named and described by Riley and Stutchbury (1836, 1840) from dinosaurian material found in the fissure fill deposit of Durdham Down in Bristol, U.K. The collection was curated in the Bristol City Museum and Art Gallery, although many of the *Thecodontosaurus* specimens were destroyed during the Second World War (Benton, 2012). Benton et al. (2000) formally described the remaining specimens and assigned them to *Thecodontosaurus antiquus*. A new specimen found in the south Wales locality of Pant-y-Ffynnon (Whiteside et al., 2016; Keeble et al., 2018) that was first interpreted as a juvenile *T. antiquus* (Kermack, 1984; Benton et al., 2000) was later assigned to a new species, *T. caducus* (Yates, 2003a), and finally to a different genus, *Pantydraco caducus* (Galton et al., 2007), based on morphological differences in the cervical vertebrae and humerus from the Durdham Down material. Additionally, an articulated pectoral girdle and forelimb (YPM 2195) from Bristol (Benton et al., 2000) was later named *Asylosaurus yalensis*, on the basis that it exhibited distinctive humeral traits (Galton, 2007). In 1975, sauropodomorph material was found in Tytherington, southwest England (Whiteside and Marshall, 2008; Whiteside et al., 2016), and since then it has been housed and prepared at the University of Bristol Geology Department (BRSUG). The new Tytherington material was later identified as *T. antiquus* (Whiteside, 1983; Galton et al., 2007), but it was never formally described. These interpretations and findings complicate the taxonomic status of *Thecodontosaurus* and apparently increase the number of sauropodomorph taxa that lived in southwestern Britain during the Late Triassic.

As it currently stands, *Thecodontosaurus* was found in two geographically close fissure localities, Durdham Down and Tytherington (Benton et al., 2000; Whiteside and Marshall, 2008; Foffa et al., 2014; Whiteside et al., 2016), which were traditionally thought to be Carnian in age. However, recent analyses of the geology and the palynology of the numerous Late Triassic

*Corresponding author.

fissure fill deposits of southwestern Britain suggest that the age of these two localities, as well as Pant-y-Ffynnon, was Rhaetian (205 Ma) instead (Whiteside et al., 2016). Their paleoenvironment has been reconstructed as small islands in a shallow sea that housed a diverse herpetofauna composed of rhynchocephalians, 'sphenosuchian' crocodylomorphs, and coelophysoid dinosaurs (Whiteside and Marshall, 2008; Foffa et al., 2014; Whiteside et al., 2016; Mussini et al., 2019). *Thecodontosaurus* was thus part of a peculiar insular ecosystem of the Late Triassic.

Here, we provide the first detailed descriptive account of the sauropodomorph material found in Tytherington and assign it to *Thecodontosaurus antiquus*. The abundant and well-preserved BRSUG collection provides new information on the osteology of the species, especially of elements of the skull that were unknown. Based on its anatomy, we discuss aspects of its paleobiology and paleoecology, including feeding and posture, and comment on the taxonomic status of Late Triassic British sauropodomorphs.

Institutional Abbreviations—**BRSMG**, Bristol City Museum and Art Gallery, Bristol, U.K.; **BRSUG**, University of Bristol Geology Department, Bristol, U.K.; **NHMUK**, Natural History Museum, London, U.K.; **PULR**, Paleontología, Universidad Nacional de La Rioja, La Rioja, Argentina; **YPM**, Yale Peabody Museum, New Haven, Connecticut, U.S.A.

MATERIALS

The *Thecodontosaurus* material from the Tytherington locality comprises over a thousand specimens housed at BRSUG. These include isolated bones or bone fragments of very disparate sizes extracted from fissure fill deposits, similar to the previously described *Thecodontosaurus* material from Durdham Down (Benton et al., 2000). Therefore, the term 'specimen' is here used to indicate an item within the BRSUG collection, as opposed to an 'individual animal.' The disarticulation of the *Thecodontosaurus* fossils from Tytherington renders the assignment of specimens to the same individual very difficult or impossible. Thus, ratios and proportions between skeletal elements are not provided in the description, despite their taxonomic importance. The anatomical description is based on the most complete specimens representing known skeletal elements and that can be confidently identified.

SYSTEMATIC PALEONTOLOGY

DINOSAURIA Owen, 1842
SAURISCHIA Seeley, 1887
SAUROPODOMORPHA Huene, 1932
THECODONTOSAURUS Riley and Stutchbury, 1836
THECODONTOSAURUS ANTIQUUS Morris, 1843
(Figs. 1–12)

Diagnosis—A sauropodomorph dinosaur distinguished from other basal sauropodomorphs by the following combination of characters (autapomorphies indicated with an asterisk): absence of a postorbital flange; maxillary and dentary tooth crowns not recurved and with coarse serrations; extensive muscle scar for the origin of M. triceps brachii caput scapulare on the lateral side of the glenoid lip of the scapula*; elaborate humeral cuboid fossa with a bilobate proximal outline and extensively pitted surface*; reduced brevis fossa and shelf; incompletely perforated acetabulum; absence of a femoral trochanteric shelf; and posterolateral descending process of the tibia anteroposteriorly wide and mediolaterally narrow, not reaching the lateral extent of the anterolateral process* (convergent with *Anchisaurus*, *Eucnemesaurus entaxonis*, *Aardonyx*, and Sauropoda).

Holotype—BRSMG Ca7465, right dentary, destroyed in 1940 (Benton et al., 2000).

Neotype—BRSMG C4529, left dentary, designated by Galton (1985).

Referred Specimens—In addition to the sauropodomorph material from Durdham Down referred to *T. antiquus* by Benton et al. (2000), over 1,000 specimens from Tytherington fissure 2 housed at BRSUG (Figs. 1–12) are here referred to this species: BRSUG 23606–BRSUG 23972, BRSUG 26585–BRSUG 26660, BRSUG 28121–BRSUG 28404, and BRSUG 29372-2805–BRSUG 29372-3812.

Locality and Horizon—Late Triassic, Rhaetian localities of Durdham Down and Tytherington fissure 2, southwestern England, U.K. (Benton et al., 2000; Whiteside and Marshall, 2008; Whiteside et al., 2016; Mussini et al., 2019).

DESCRIPTION

Skull

Maxilla—A posterior portion of a left maxilla was found in Tytherington (Fig. 1A, B). The lateral surface preserves the two posterior-most lateral foramina. The posterior maxillary foramen is the most notable in size and is placed at the anterior end of an anteroposteriorly elongated groove, as seen in *Saturnalia* (Bronzati et al., 2019). The ventral surface bears a series of seven posterior alveoli that are small, circular, and closely packed, with very thin interalveolar walls. The ventral surface of the maxilla medial to the tooth row presents numerous minute pits. Only one tooth, attached to the anterior-most alveolus, is preserved (Fig. 1C). It has a small, lanceolate crown with coarse serrations (5 per mm) oblique to the carina and the apicobasal axis of the tooth. The crown is labiolingually compressed and not curved. The crowns are basally constricted. The root is deep and straight. Tooth morphology is very similar to that of the dentary teeth of the *T. antiquus* neotype (Benton et al., 2000) and *Pantydraco* (Galton and Kermack, 2010) but differs from dentary tooth morphology of more basal taxa such as *Buriolestes* (Müller et al., 2018c), *Saturnalia* (Bronzati et al., 2019), and *Eoraptor* (Sereno et al., 2013), which have curved and finely serrated teeth.

Squamosal—Tytherington yielded a right squamosal that is missing the anterior portion (Fig. 1D, E). The medial surface is marked by a semispherical quadrate cotyle for reception of the quadrate head. The quadrate cotyle is dorsally roofed by the squamosal main body, which presents a medial concave and anteroposteriorly elongated surface, laterally bounded by a ridge, which represents the parietal articular surface. The quadrate ramus is straight and directed anteroventrally, tapers ventrally, and bears a medial groove. The medial ramus is directed posteromedially; it is short and acute, with a triangular cross-section.

Frontal—A complete right frontal (Fig. 1F, G) and an incomplete right frontal are preserved. The bone is dorsoventrally flat, and its dorsal and ventral surfaces are smooth. The frontal is longer than wide and has a similar mediolateral width throughout its length, unlike other sauropodomorphs such as *Saturnalia* (Bronzati et al., 2019) and *Panphagia* (Martínez et al., 2012), in which the bone notably increases in width posteriorly. In dorsal view (Fig. 1F), the frontal presents a deep, anterolateral 'V'-shaped fossa, with the apex directed posteriorly, which corresponds to the prefrontal articular surface. Anteromedial to the prefrontal articular surface, representing the anterior end of the bone, a concavity marks the nasal articular surface. The lateral margin of the bone posterior to the prefrontal articular surface is concave and represents the orbital rim. The medial margin of the bone is slightly projected dorsally, forming the frontal medial crest along the suture with the left counterpart. Contribution of the frontal to the supratemporal fossa, lost in sauropods (Wilson, 2002), cannot be confirmed because the posterolateral corner of the bone is obscured by matrix. A laterally concave, ventrally projecting ridge is present on the ventral surface of the frontal (Fig. 1G). This is the orbital margin, and the surface

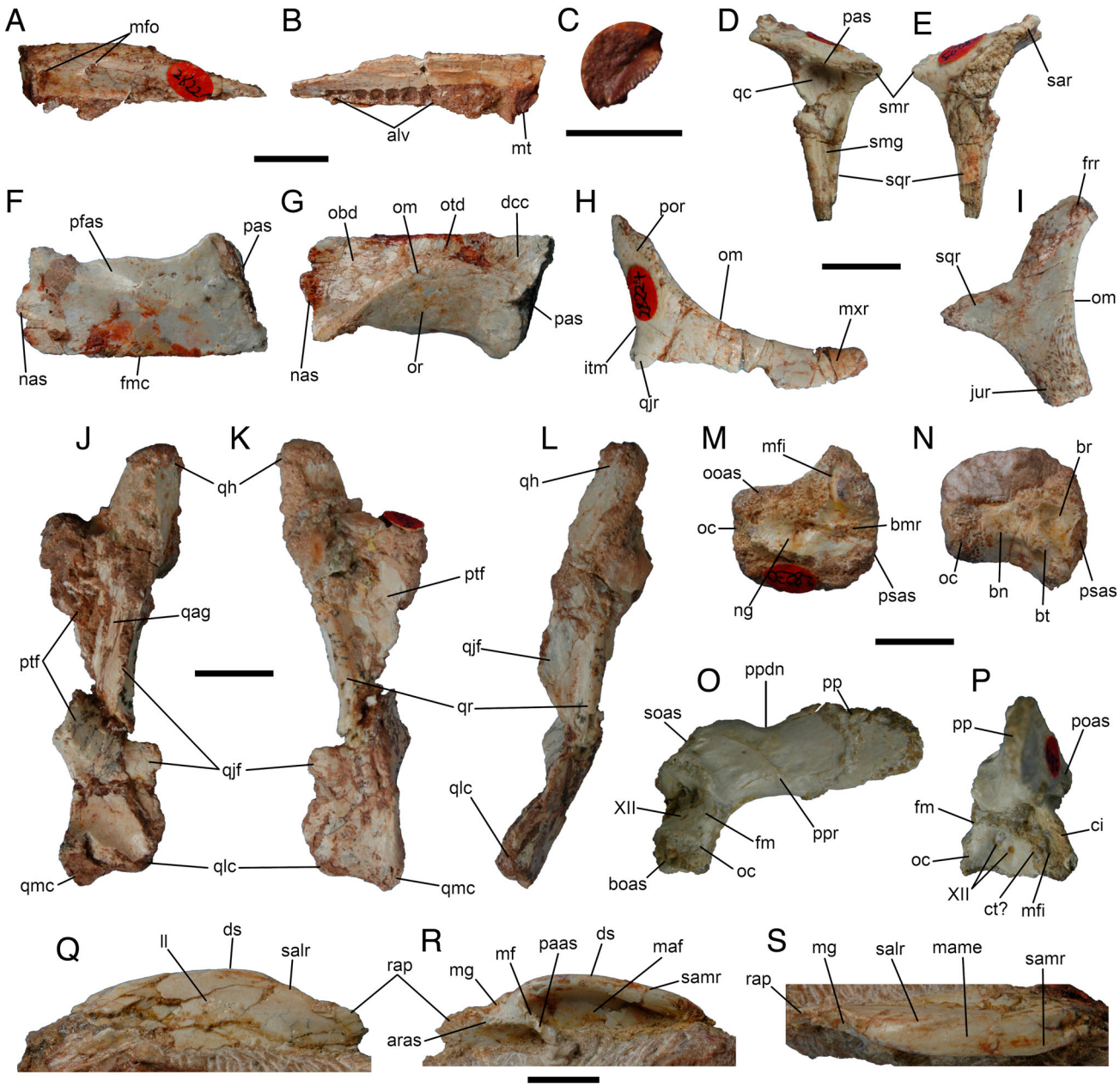

FIGURE 1. *Thecodontosaurus antiquus*, skull bones. **A**–**C**, BRSUG 28221, left maxilla in **A**, lateral and **B**, ventral views, and **C**, close-up of the maxillary tooth. **D**, **E**, BRSUG 28223, left squamosal in **D**, medial and **E**, lateral views. **F**, **G**, BRSUG 29372-2855, left frontal in **F**, dorsal and **G**, ventral views. **H**, BRSUG 28224, left jugal in lateral view. **I**, BRSUG 26660, left postorbital in lateral view. **J**–**L**, BRSUG 26596, left quadrate in **J**, anterior, **K**, posterior, and **L**, lateral views. **M**, **N**, BRSUG 28230, basioccipital in **M**, dorsal and **N**, ventral views. **O**, **P**, BRSUG 28234, right otoccipital in **O**, posterior and **P**, lateral views. **Q**–**S**, BRSUG 28201, left surangular in **Q**, lateral, **R**, medial, and **S**, dorsal views. **Abbreviations**: **alv**, alveoli; **aras**, articular articular surface; **bmr**, basioccipital median ridge; **bn**, basioccipital neck; **boas**, basioccipital articular surface; **br**, basioccipital recess; **bt**, basal tubera; **ci**, crista interfenestralis; **ct**, crista tuberalis; **dcc**, dorsal roof of cerebral cavity; **ds**, dorsal shelf; **fm**, foramen magnum; **fmc**, frontal medial crest; **frr**, frontal ramus; **itm**, margin of the infratemporal fenestra; **jur**, jugal ramus; **ll**, lateral lamina; **mame**, M. adductor mandibulae externus (mAME) insertion; **maf**, mandibular adductor fossa; **mf**, medial flange; **mfi**, metotic fissure; **mfo**, maxillary foramina; **mg**, mandibular glenoid; **mt**, maxillary tooth; **mxr**, maxillary ramus; **nas**, nasal articular surface; **ng**, neural groove; **obd**, olfactory bulb depression; **oc**, occipital condyle; **om**, orbital margin; **ooas**, otoccipital articular surface; **or**, orbital roof; **otd**, olfactory tract depression; **paas**, prearticular articular surface; **pas**, parietal articular surface; **pfas**, prefrontal articular surface; **poas**, prootic articular surface; **por**, postorbital ramus; **pp**, paraoccipital process; **ppdn**, dorsal notch; **ppr**, paraoccipital process ridge; **psas**, parabasisphenoid articular surface; **ptf**, pterygoid flange of quadrate; **qag**, quadrate anterior groove; **qc**, quadrate cotyle; **qh**, quadrate head; **qjf**, quadratojugal flange of quadrate; **qjr**, quadratojugal ramus; **qlc**, quadrate lateral condyle; **qmc**, quadrate medial condyle; **qr**, quadrate ridge; **rap**, retroarticular process; **salr**, surangular lateral ridge; **samr**, surangular medial ridge; **sar**, squamosal anterior ramus; **smg**, squamosal medial groove; **smr**, squamosal medial ramus; **soas**, supraoccipital articular surface; **sqr**, squamosal quadrate ramus; **XII**, cranial nerve XII (hypoglossal) foramina. Scale bars equal 1 cm (**A**, **B**, **D**–**S**) and 5 mm (**C**).

lateral to it forms the orbital roof and slopes dorsally in a lateral direction. Medial to the orbital margin, the ventral surface is depressed. The posterior part of the ventral surface shows an anteroposteriorly elongated oval fossa that corresponds to the cerebral cavity. The cerebral cavity depression is continued anteriorly by a laterally narrow olfactory tract depression that dorsally bounded the olfactory tract. As in *Massospondylus* (Chapelle and Choiniere, 2018), this is the shallowest part of the depression. This continues with the anterior portion of the medial depression, represented by the olfactory bulb depression. Unlike in *Macrocollum* (Müller, 2020), this depression is not medially bounded by a crest. In lateral view, the orbital margin is almost straight, unlike in other sauropodomorphs in which it is dorsally convex, such as *Pantydraco* (Galton and Kermack, 2010) and *Massospondylus* (Chapelle and Choiniere, 2018).

Jugal—A single specimen representing a right jugal is known (Fig. 1H). The jugal is triradiate and forms the posteroventral and ventral margins of the orbit, the infraorbital bar, and the anterior portion of the infratemporal bar. The jugal is not straight in anterior view, because the postorbital ramus curves laterally with respect to the jugal main body. The postorbital ramus is relatively short and posterodorsally oriented. Its dorsal end articulates with the jugal ramus of the postorbital by a larger anterior fossa ventrally delimited by a mediolaterally oriented ridge, and a smaller posteromedial fossa. The orbital margin of the jugal laterally bounds a flat anteromedially oriented surface that represents the anterodorsal surface of the bone and the postorbital articular surface.

Postorbital—A left postorbital is known, which has its three rami tips broken (Fig. 1I). The bone is triradiate and forms the posterior margin of the orbit. The anterior surface is flat, separated from the medial and lateral surfaces of the bone by two marked rims, making the jugal ramus triangular in cross-section. The postorbital lacks an orbital flange, unlike other basal sauropodomorphs (Galton and Kermack, 2010; Yates et al., 2011; Sereno et al., 2013; Müller et al., 2018c; Bronzati et al., 2019; Langer et al., 2019; Müller, 2020). This flange is reduced or absent in other, particularly more derived, sauropodomorphs, such as *Plateosaurus* (Prieto-Márquez and Norell, 2011), *Massospondylus* (Chapelle and Choiniere, 2018), and *Adeopapposaurus* (Martínez, 2009). The frontal ramus is robust but anteromedially compressed. Its lateral surface presents multiple pits and grooves. The squamosal ramus forms the anterior portion of the supratemporal bar. It is mediolaterally compressed, and its anteroventral surface, dorsal to the posterodorsal end of the jugal ramus, presents a small fossa bounded by a lateral ridge.

Quadrate—Only a left quadrate is known from Tytherington, which exhibits the typical columnar, dorsoventrally elongated morphology of early dinosaurs (Fig. 1J–L). The main body of the quadrate has a gentle sigmoid shape in lateral view (Fig. 1L), but less curved than in *Macrocollum* (Müller, 2020). The quadrate head is ellipsoid in dorsal view, with a mediolateral long axis. Both the quadratojugal and pterygoid flanges have their anterior tips broken. Thus, the presence of a quadrate foramen cannot be determined. The medial pterygoid flange projects anteromedially and the quadratojugal flange anterolaterally. Both are laminar and delimit a dorsoventrally elongated anterior groove. The pterygoid flange is taller, reaching a more dorsal position. The lateral surface of the quadratojugal ramus is concave and posteriorly bounded by a marked quadrate ridge that runs along the posterior surface of the bone. The ventral end bears the quadrate condyles, of which the medial condyle projects more ventrally. In ventral view, the medial condyle is more anteroposteriorly elongated, whereas the lateral one is rounded and dome-shaped. The two quadrate condyles are separated by an anteromedially oriented groove.

Basioccipital—The basioccipital forms the ventral margin of the foramen magnum and the posterior floor of the endocranial cavity (Fig. 1M, N). The dorsal surface is marked by an anteroposterior groove running along the parasagittal plane from the foramen magnum, which represents the neural or medullar groove. The neural groove is bounded on both sides by pitted and rugose surfaces, the left and right otoccipital articular surfaces. A median ridge splits the neural groove into two at the anterior third of the bone, as seen in YPM 2192 and in other early dinosaurs such as *Pantydraco* (Galton and Kermack, 2010) and *Lesothosaurus* (Porro et al., 2015). The metotic fissure is preserved on the left side of the dorsal surface of the bone, branching perpendicular to the neural groove. It is similarly laterally elongated and anteroposteriorly narrower to that of YPM 2192 and *Pantydraco* (Galton and Kermack, 2010). The basal tubera are prominent and anterolaterally oriented ridges with knob-like medial ends. The lateral portion of the basal tubera is less robust than in *Macrocollum* (Müller, 2020). A mediolaterally oriented ridge connects the paired basal tubera. A deep basisphenoid recess is present anterior to the basal tubera and posterior to the basioccipital-basisphenoid suture, as in *Efraasia* (Bronzati and Rauhut, 2018), *Unaysaurus* (McPhee et al., 2019), and *Massospondylus* (Chapelle and Choiniere, 2018), among others. The occipital condyle is knob-shaped, and its ventral projection is not notably marked due to weathering. In ventral view (Fig. 1N), the occipital condyle is anteroposteriorly longer than those of *Saturnalia* (Bronzati et al., 2019), *Efraasia* (Bronzati and Rauhut, 2018), and *Adeopapposaurus* (Martínez, 2009), but similar to that of YPM 2192 (Benton et al., 2000). The occipital condyle and the basal tubera are connected by the biconcave basioccipital neck.

Otoccipital—The otoccipital exhibits the usual triradiate morphology, with a lateral paraoccipital process, a ventral pyramidal projection (sensu Bronzati and Rauhut, 2018), and an anteroventral crista interfenestralis (Fig. 1O, P). The paraoccipital process is elongated and posterolaterally directed, as seen in *Pantydraco* (Galton and Kermack, 2010) and *Adeopapposaurus* (Martínez, 2009) and in the braincase (YPM 2192) of the Durdham Down *T. antiquus* (Benton et al., 2000). It is dorsoventrally widest at its mediolateral midpoint, and its lateral end has a rounded outline in anterior view. The posterior surface of the paraoccipital process is marked by an oblique, ventrolaterally oriented, dorsolaterally curved ridge. This delimits ventrally a concave surface where neck muscles would have attached. The anterior surface of the paraoccipital process is marked by a proximal semicircular area with multiple mediolaterally oriented ridges that represent the prootic articular surface. The dorsal surface of the paraoccipital process shows a notch that might represent the posterior border of the posttemporal foramen, a derived trait present in *Pantydraco* (Galton and Kermack, 2010), *Macrocollum*, and more derived sauropodomorphs (Müller, 2020). On the lateral side of the bone (Fig. 1P), ventral to the paraoccipital process, two posterior foramina representing the openings for cranial nerve XII (hypoglossal) are present. The posterior-most of the two is the largest, oval, and more dorsally positioned. Both openings have their medial counterparts on the posteroventromedial surface of the otoccipital. Anterodorsal to the cranial nerve XII foramina, there is a large, dorsoventrally elongated opening infilled with matrix that probably represents the metotic fissure. This opening is the exit for cranial nerves IX, X, and XI and is not subdivided, as in YPM 2192 (Benton et al., 2000), *Plateosaurus* (Prieto-Márquez and Norell, 2011), and *Massospondylus* (Chapelle and Choiniere, 2018) but unlike in most basal sauropodomorphs (Bronzati and Rauhut, 2018). The metotic fissure is anteriorly bounded by a tall, posterodorsally inclined crista interfenestralis (= metotic crest). This ramus separates the metotic fissure from the foramen ovale. The metotic fissure seems to be posteriorly bounded by a crista tuberalis, although this part of the bone is abraded. The posteroventral end of the pyramidal projection forms the dorsolateral portion of the occipital condyle. The posterodorsal surface of the

otoccipital is rugose and pitted and represents the supraoccipital articular surface.

Mandible

Surangular—The incomplete left surangular is missing its anterior portion (Fig. 1Q–S). The surangular is mediolaterally flat and dorsally convex in lateral view. The dorsal shelf is dorsolaterally flattened, lacking a coronoid process. Its dorsal surface is smooth and medially bounded by a medial ridge, representing the insertion site of the M. adductor mandibulae externus complex (Holliday, 2009). Posterolaterally to the muscle attachment area, a lateral ridge extends to the posterior end of the shelf. Posterior to the dorsal shelf, the surangular decreases in dorsoventral depth, forming a dorsally concave margin that continues posteriorly with the broken posterodorsally oriented retroarticular process. The medial portion of the bone houses the adductor fossa, insertion site for M. adductor mandibulae profundus and M. pseudotemporalis complexes (Holliday, 2009), which are laterally bounded by the lateral lamina, dorsally by the dorsal shelf, and posteriorly by the medial flange. It is open medially through the internal mandibular fenestra. The medial flange is a medial protrusion of the surangular, with a triradiate shape in medial view. Its anteroventral extension, which forms the posterior wall of the adductor fossa, would articulate medially with the prearticular. Its posterior ramus presents a medioventrally facing articular surface for the articular. The dorsal portion of the medial flange is dorsomedially concave and forms the anterior part of the mandibular glenoid.

Axial Skeleton

Atlas—A right atlantal neurapophysis is known from Tytherington (Fig. 2A, B), which has a similar morphology to those of other basal sauropodomorphs such as *Adeopapposaurus* (Martínez, 2009) and *Leyesaurus* (Apaldetti et al., 2011). The anterior-most feature is the pedicle, which is ventromedially oriented and has a reniform end, the dorsal portion of which represents the occipital condyle articular surface and the ventral portion represents the atlantal intercentrum articular surface. The prezygapophysis is anteromedially directed and is formed by a thick lamina. The broken postzygapophysis is placed posterior to it and is thinner than the anterior zygapophysis. A shallow dorsal depression is present on the lateral wall of the postzygapophysis and of the posterior portion of the prezygapophysis. This depression is ventrally bounded by a keel that extends posteriorly to form the posteriorly directed, spear-shaped epipophysis.

Cervical Vertebrae—Few postaxial cervical vertebrae have been found at Tytherington, none of them in articulation. Anterior cervical vertebrae are elongated, dorsoventrally short, and mediolaterally narrow (Fig. 2C). The neural spine is dorsoventrally short and mediolaterally thin. The zygapophyses are horizontal and extend anterior and posterior to the neural arch and the centrum. The prezygapophyses are dorsomedially oriented and are separated by a deep, anteroposteriorly elongated spinoprezygapohyseal fossa (sensu Wilson et al., 2011). The postzygapophyses face ventrolaterally and are separated by a deep spinopostzygapohyseal fossa that seems to penetrate superficially below the neural spine (Fig. 2D). The epipophyses are abraded in almost all specimens, but the left epipophysis in BRSUG 29372-2842 is plate-like and reaches the posterior end of the postzygapophysis. The position and morphology of the diapophyses vary between cervical vertebrae. In more anterior cervical vertebrae, the diapophyses are anteriorly positioned, elongated, and slightly projected laterally. In more posterior cervicals (Fig. 2E–H), the diapophyses are placed more toward the vertebral midlength and are aliform and project laterally. This variation is seen in other sauropodomorphs such as *Adeopapposaurus* (Martínez, 2009) and *Leonerasaurus* (Pol et al., 2011). The anterior and posterior openings of the neural canal are elliptical, wider than tall. The zygodiapophyseal table is separated from the centrum by a dorsally convex keel. The centra are amphicoelous and constricted dorsoventrally and mediolaterally at midlength; they are approximately three times longer than tall. In ventral view (Fig. 2G), the anterior end of the centrum is mediolaterally wider than the posterior because of the circular parapophyses. There is an anteroposteriorly oriented ventral keel, most developed toward the anterior end, as well as anteroposterior striations on the ventral centrum. The neural spine in the posterior-most cervical vertebrae is anteroposteriorly shorter than in anterior and middle cervicals. The prezygapophyeses are relatively shorter, not extending much anterior to the centrum, and the postzygapophyses are not horizontal but project posterodorsally. The diapophyses are more elongated and aliform, projecting ventrolaterally.

Dorsal Vertebrae—Vertebral elements of the trunk (Fig. 2I–N) belong to middle or posterior dorsals, which are not preserved in articulation. Neural spines are broken in most specimens except for a posterior dorsal (Fig. 2N), in which this structure is subrectangular in lateral view and subequal in dorsoventral height to the rest of the neural arch. The shapes of the neural canal anterior and posterior openings differ, the former being subcircular in outline and the latter being dorsoventrally tall and slot-shaped (Fig. 2J, K). The diapophyses are directed laterally, as in other basal sauropodomorphs, with a slight dorsal component in some specimens (Fig. 2L). The prezygapophyses are short, hardly extending anterior to their respective centrum in posterior dorsals (Fig. 2I, N). Their articular facets are oval and directed mediodorsally. The spinoprezygapohyseal fossa is reduced to a small ellipsoid depression (Fig. 2J). The postzygapophyses project posteriorly, extending beyond the posterior margin of the centrum, unlike the prezygapophyses. A narrow, dorsoventrally high spinopostzygapophyseal fossa is present in between. The zygapophyses bear hyposphene-hypantrum articulations (Fig. 2I–K, N). The hypantrum is present as an anteroposterior groove on the ventromedial side of the prezygapophysis. The hyposphene results from a ventral projection of the postzygapophysis, and its dorsoventral height is less than that of the neural canal, as is common in basal sauropodomorphs. The postzygapophysis and the hyposphene delimit a laterally concave fossa that serves for reception of the prezygapophysis of the vertebra immediately behind. This fossa is anteroventrally separated from the posterior infradiapophyseal fossa (sensu Yates et al., 2012) by an accessory lamina. The centrodiapophyseal fossa is triangular in lateral view and located ventral to the diapophysis. This fossa is posteriorly bounded by the posterior centrodiapophyseal lamina and, in posterior dorsal vertebrae, anteriorly delimited by the parapophysis and a short paradiapophyseal lamina. The well-developed postzygodiapophyseal and posterior centrodiapophyseal laminae dorsally and anteriorly bound the deep posterior infradiapophyseal fossa, respectively. The parapophyses are fully located on the neural arch in all specimens, well separated from the centrum by anterior centroparapophyseal laminae (sensu Wilson et al., 2011). The articular surface of the parapophyses is subcircular in outline and concave (Fig. 2L). The neurocentral sutures are visible in all specimens. The relative length of the centrum varies among dorsal vertebrae, from 1.1 to 1.6 times the centrum height. Dorsal centra are amphicoelous to amphiplatyan and bear an anteroposteriorly elongated lateral depression. In lateral view, the ventral margin of the centrum is strongly concave, with anterior and posterior ends extending further ventrally than at the center.

Sacral Vertebrae—Two sacral vertebrae have been found at Tytherington: a relatively complete second primordial (Fig. 3A–D) and a very fragmentary centrum. The centrum morphology

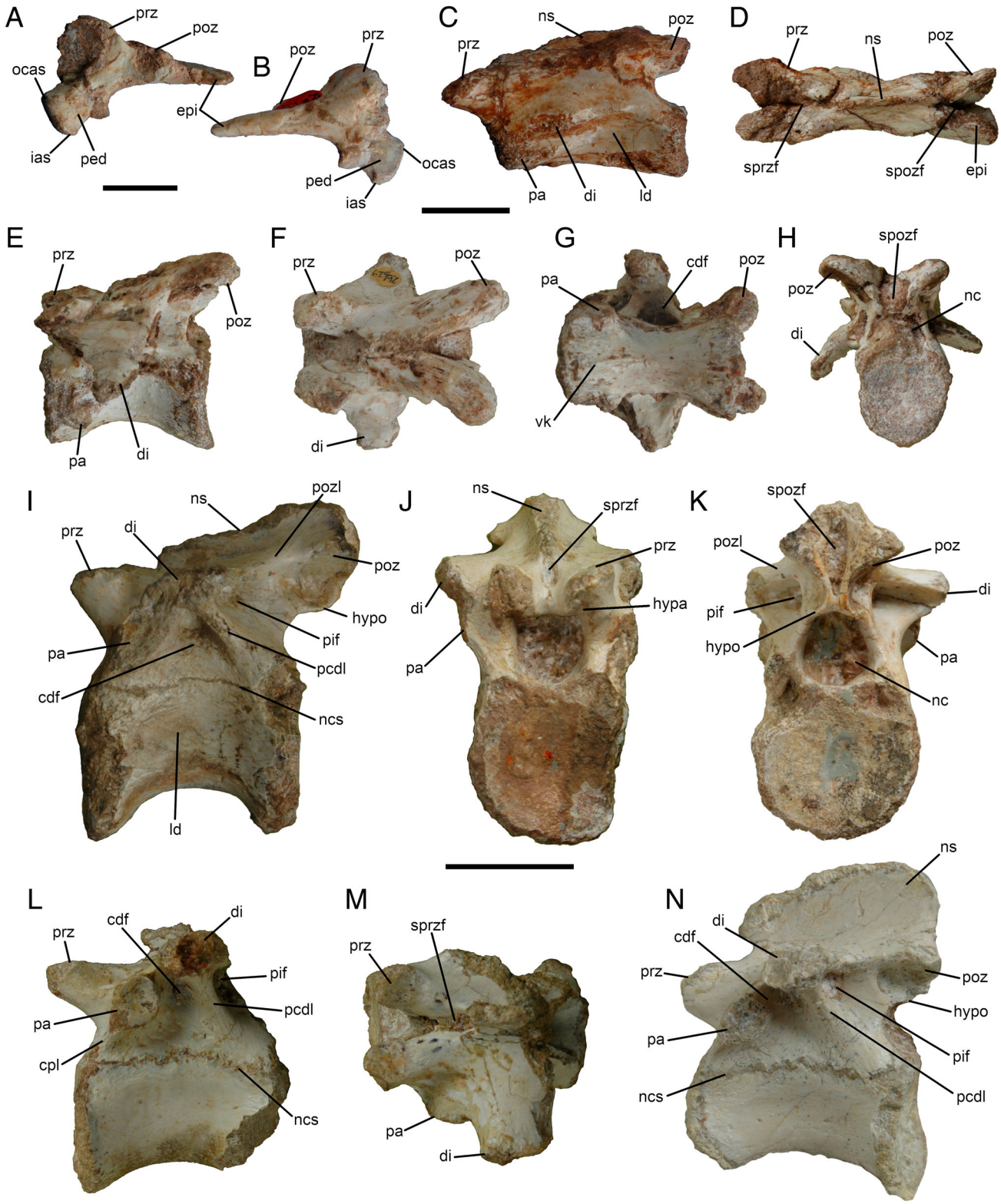

FIGURE 2. *Thecodontosaurus antiquus*, cervical and dorsal vertebrae. **A**, **B**, BRSUG 28198, right atlantal neurapophysis in **A**, medial and **B**, lateral views. **C**, BRSUG 28124, middle cervical vertebra in lateral view. **D**, BRSUG 29372-2842, mid-cervical neural arch in dorsal view. **E**–**H**, BRSUG 26629, posterior cervical vertebra in **E**, left lateral, **F**, dorsal, **G**, ventral, and **H**, posterior views. **I**–**K**, BRSUG 29372-3811, posterior dorsal vertebra in **I**, left lateral, **J**, anterior, and **K**, posterior views. **L**, **M**, BRSUG 29372-2806, middle dorsal vertebra in **L**, left lateral and **M**, dorsal views. **N**, BRSUG 29372-2848, posterior dorsal vertebra in left lateral view. **Abbreviations**: **cdf**, centrodiapophyseal fossa; **cpl**, centroparapophyseal lamina; **di**, diapophysis; **epi**, epipophysis; **hypa**, hypantrum; **hypo**, hyposphene; **ias**, intercentrum articular surface; **ld**, lateral depression; **nc**, neural canal; **ncs**, neurocentral suture; **ns**, neural spine; **ocas**, occipital articular surface; **pa**, parapophysis; **pcdl**, posterior centrodiapophyseal lamina; **ped**, pedicle; **pif**, posterior infradiapophyseal fossa; **poz**, postzygapophysis; **pozl**, postzygodiapophyseal lamina; **prz**, prezygapophysis; **spozf**, spinopostygapophyseal fossa; **sprzf**, spinoprezygapophyseal fossa; **vk**, ventral keel. Scale bars equal 1 cm (**A, B**) and 2 cm (**C**–**N**).

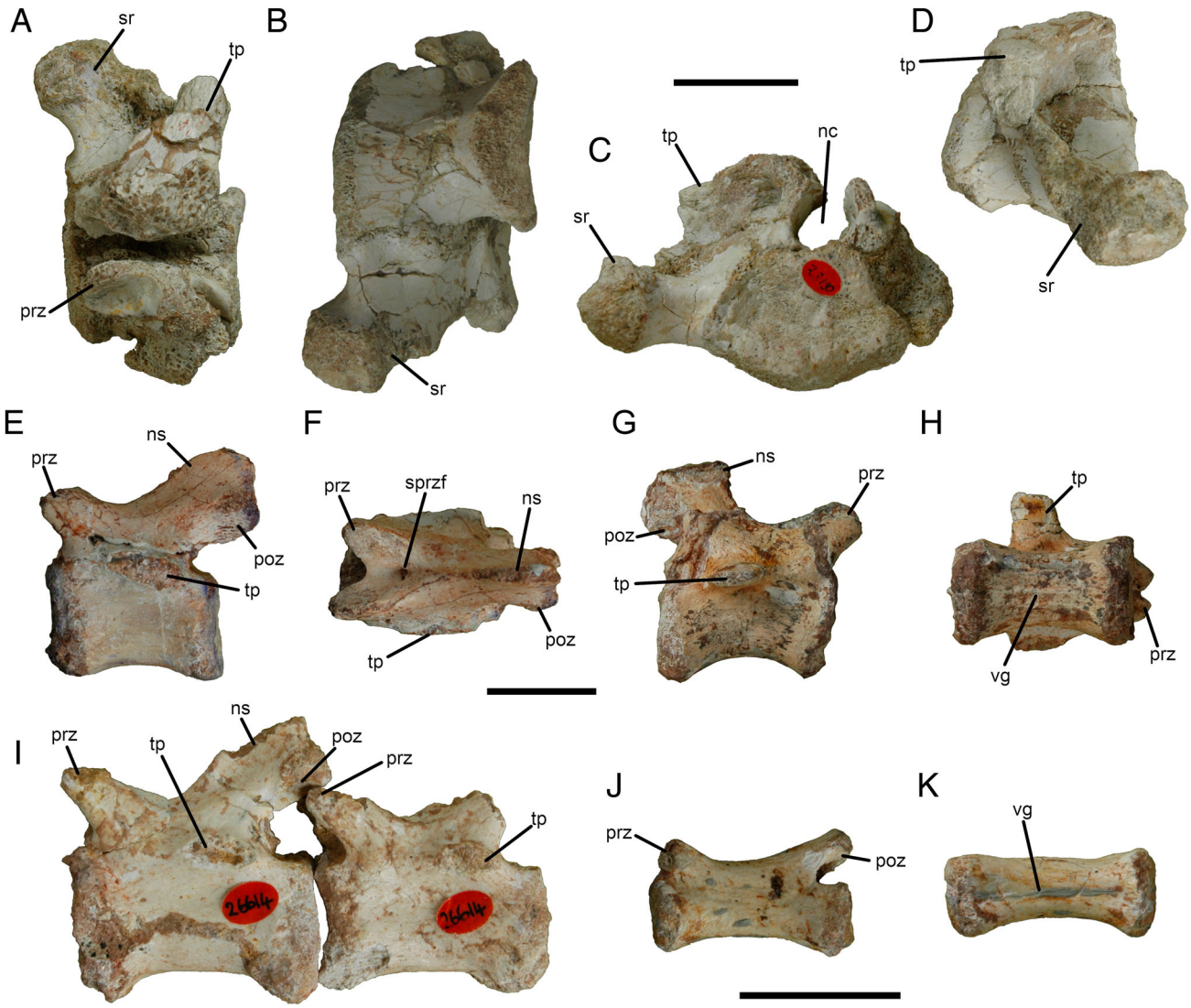

FIGURE 3. *Thecodontosaurus antiquus*, sacral and caudal vertebrae. **A**–**D**, BRSUG 28130, second sacral vertebra in **A**, dorsal, **B**, ventral, **C**, anterior, and **D**, right lateral views. **E**, **F**, BRSUG 29372-2843, mid-anterior caudal vertebra in **E**, left lateral and **F**, dorsal views. **G**, **H**, BRSUG 29372-2830, middle caudal vertebra in **G**, right lateral and **H**, ventral views. **I**, BRSUG 26614, two articulated middle caudal vertebrae in left lateral view. **J**, **K**, BRSUG 29372-2812, mid-posterior caudal vertebra in **J**, left lateral and **K**, ventral views. **Abbreviations**: **nc**, neural canal; **ns**, neural spine; **poz**, postzygapophysis; **prz**, prezygapophysis; **sprzf**, spinoprezygapophyseal fossa; **sr**, sacral rib; **tp**, transverse process; **vg**, ventral groove. Scale bars equal 2 cm.

of the second primordial in anterior and posterior views is an isosceles trapezoid with a convex ventral side. The length of the second sacral centrum is 1.7 times its dorsoventral height and equal to its transverse width. The anterior articular surface of the centrum is wider and taller than the posterior one. The second sacral rib has a ventrally positioned anterior iliac contact that curves dorsally in a posterior direction to contact the transverse process, forming an anterodorsally concave outline. The anterior portion of the sacral rib contacts the sacral centrum, whereas the posterior one articulates with the transverse process of the neural arch, which is broken. This condition supports the identification of this element as a second primordial sacral. In dorsal view (Fig. 3A), the distal portion of the sacral rib expands anterioposteriorly to contact the ilium and its anterior end is notably robust. The neural spine and most of the neural arch is not preserved. The neural canal is wide, contributed by a sulcus on the dorsal surface of the centrum, which left space for a lumbar enlargement of the spinal cord. No articulated sacrum is preserved, but the sacral rib articular surface of the ilium (see Fig. 9B) suggests the presence of two primordial sacral vertebrae. Evidence for additional sacral vertebrae is unclear (see Ilium section).

Caudal Vertebrae—Multiple isolated caudals from different positions in the tail were found at Tytherington (Fig. 3E–K). The caudal centra become progressively more elongated and dorsoventrally shorter posteriorly along the tail, from a length-to-height ratio of 1.4 in proximal elements to 3.4 in posterior ones. The transverse processes are lenticular in proximal cross-section (Fig. 3E, G). The only well-preserved transverse process corresponds to a mid-anterior vertebra (Fig. 3H). This process is plate-like, horizontal, and posterolaterally oriented. The neural spines are not completely preserved and are located on the

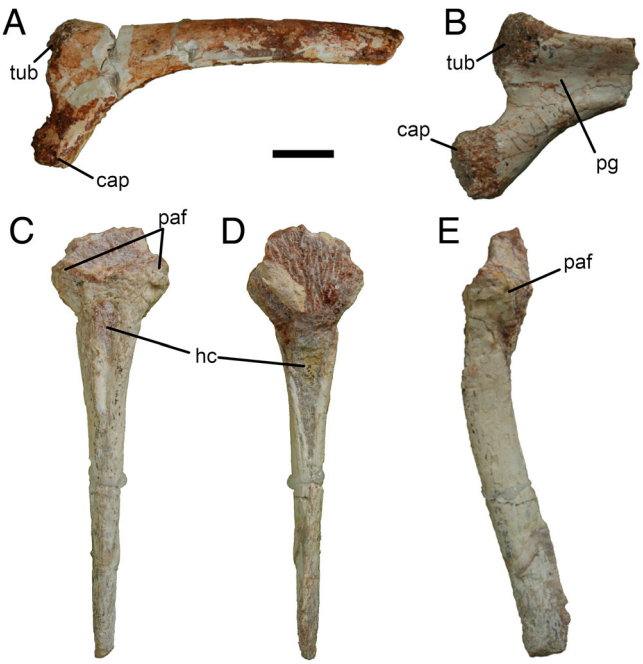

FIGURE 4. *Thecodontosaurus antiquus*, dorsal ribs and chevron. **A**, BRSUG 29372-3595, proximal portion of left dorsal rib in anterior view. **B**, BRSUG 29372-3592, head of right dorsal rib in ventral view. **C**–**E**, BRSUG 29372-3285, chevron in **C**, anterior, **D**, posterior, and **E**, left lateral views. **Abbreviations**: **cap**, capitulum; **hc**, hemal canal; **paf**, proximal articular facets; **pg**, posterior groove; **tub**, tuberculum. Scale bar equals 1 cm.

posterior half of the neural arch. Anteriorly, the neural spine turns into a dorsal ridge that bifurcates to meet both prezygapophyses (Fig. 3F). The laterally projecting prezygapophyses are anterodorsally oriented and slightly exceed the anterior end of the centrum, whereas the postzygapophyses project posterodorsally beyond the posterior end of the centrum. This condition is similar to that in *Adeopapposaurus* (Martínez, 2009), but in *Pampadromaeus* it is the prezygapophyses that surpass the end of the centra (Langer et al., 2019). As in most basal sauropodomorphs, the postzygapophyses are located on both sides of the posterior portion of the base of the neural spine. The articular surfaces of the pre- and postzygapophyses face dorsomedially and ventrolaterally, respectively. In anterior to middle caudals, the space between the prezygapophyses delimits a 'V'-shaped spinoprezygapophyseal fossa that terminates posteriorly in a subcircular hole (Fig. 3F). The spinopostzygapophyseal fossa is a dorsoventrally oriented slit located posteroventrally to the base of the neural spine. The neural canal is cylindrical along the caudal series, becoming slightly dorsoventrally compressed in the posterior-most caudals. The articular surfaces of the centra are amphicoelous. The ventral surface of the centrum presents a reduced anteroposterior groove that extends from end to end and is bounded laterally by ridges (Fig. 3H). The posterior ends of the centra bear two ventral condyles on both sides of the longitudinal sulcus that articulate with the chevrons. The posterior caudals have rod-like centra and lack transverse processes (Fig. 3J, K). The neural spine is reduced to a posterior ridge on the neural arch, or absent in the posterior-most elements. The articular surfaces of the prezygapophyses face medially, and those of the postzygapophyses are directed laterally.

Dorsal Ribs—Dorsal ribs are slender elements of which only proximal fragments are preserved (Fig. 4A, B). The shaft presents a gentle curvature, with a greater medial inflection immediately distal to the tuberculum-capitulum junction. The capitulum and the tuberculum delimit a 'U'-shaped medial margin of the rib head. The capitulum is twice the length of the tuberculum, and it is mediolaterally broader. It is slightly constricted at the base and expands medially to form a hemispherical head. The shaft of the dorsal ribs is ovoid in cross-section, as in *Pampadromaeus* (Langer et al., 2019), anteroposteriorly flattened and with a sharp lateral edge. The posterior surface of the shaft bears a lateral groove that runs distally from the tuberculum-capitulum junction.

Chevrons—Three complete chevrons are preserved, which vary in length from 2.4 to 6.5 cm. Chevrons present the usual 'Y'-shaped morphology (Fig. 4C–E). The proximal articulations for the caudal centra contact at the sagittal plane, with no signs of dorsal opening of the hemal canal. The proximal articular facets delimit a concave surface in anterior view, with lateral flanks that extend dorsally contacting the ventral and ventrolateral margins of the centrum ends. The hemal canal openings differ, the anterior being proximodistally shorter than the posterior. The anterior opening is a mediolaterally narrow slit, and the posterior one is triangular, proximodistally elongated and mediolaterally narrow, both being proximally broader and tapering distally. One-third along their length, the chevrons curve from a ventral-to-posteroventral orientation. The distal portion of the chevron is mediolaterally flattened and of similar anteroposterior width, without a distal expansion.

Appendicular Skeleton

Scapula—Several scapulae have been found at Tytherington, most of them fragmentary but well preserved and only one being essentially complete (Fig. 5C, D). The scapular blade is narrow and elongated, with parallel dorsal and ventral margins. It is arched laterally and does not expand significantly at its posterior end, differing from the condition in other basal members of Sauropodomorpha such as *Saturnalia* (Langer et al., 2007) and *Panphagia* (Martínez and Alcober, 2009). The body of the scapula is dorsoventrally tall compared with the blade. The dorsal and ventral margins expand gradually from the neck, unlike in *Eoraptor* (Sereno et al., 2013), *Saturnalia* (Langer et al., 2007), and *Panphagia* (Martínez and Alcober, 2009), in which they form almost right angles. The acromial (dorsal) half of the body is mediolaterally narrow and plate-like, with a sharp edge, compared with the robust glenoid (ventral) half. The scapular lateral fossa is large and shallow, and it is bounded by a low acromial ridge. This fossa represents the scapular origin of M. supracoracoideus (Otero, 2018). The lateral surface of the glenoid lip bears a muscle scar in the form of a rugose oval buttress (Fig. 5A) that indicates the origin of M. triceps brachii caput scapulare (Otero, 2018). Such an extensive scar is not present in any other basal sauropodomorph (Langer et al., 2007, 2019; Martínez and Alcober, 2009). The lateral surface of the acromion posterior to the lateral fossa exhibits numerous deep and wide pits that are a muscle scar left by the origin of M. deltoideus clavicularis. The medial surface of the scapular blade shows a ventromedial ridge extending posteriorly from the glenoid lip (Fig. 5B). The surface between this ridge and the sharp ventral border of the blade is grooved and served as the origin of M. scapulohumeralis posterior. Dorsal to the ventromedial ridge, the medial longitudinal fossa with surface pitting marks the origin of M. subscapularis (Otero, 2018).

Coracoid—Only one coracoid specimen was found, which represents the posteroventral part of a right coracoid, including the glenoid and the coracoid foramen (Fig. 5E–G). The coracoid has a concave medial surface and a convex lateral surface. The coracoidal glenoid surface is abraded, but this part of the bone

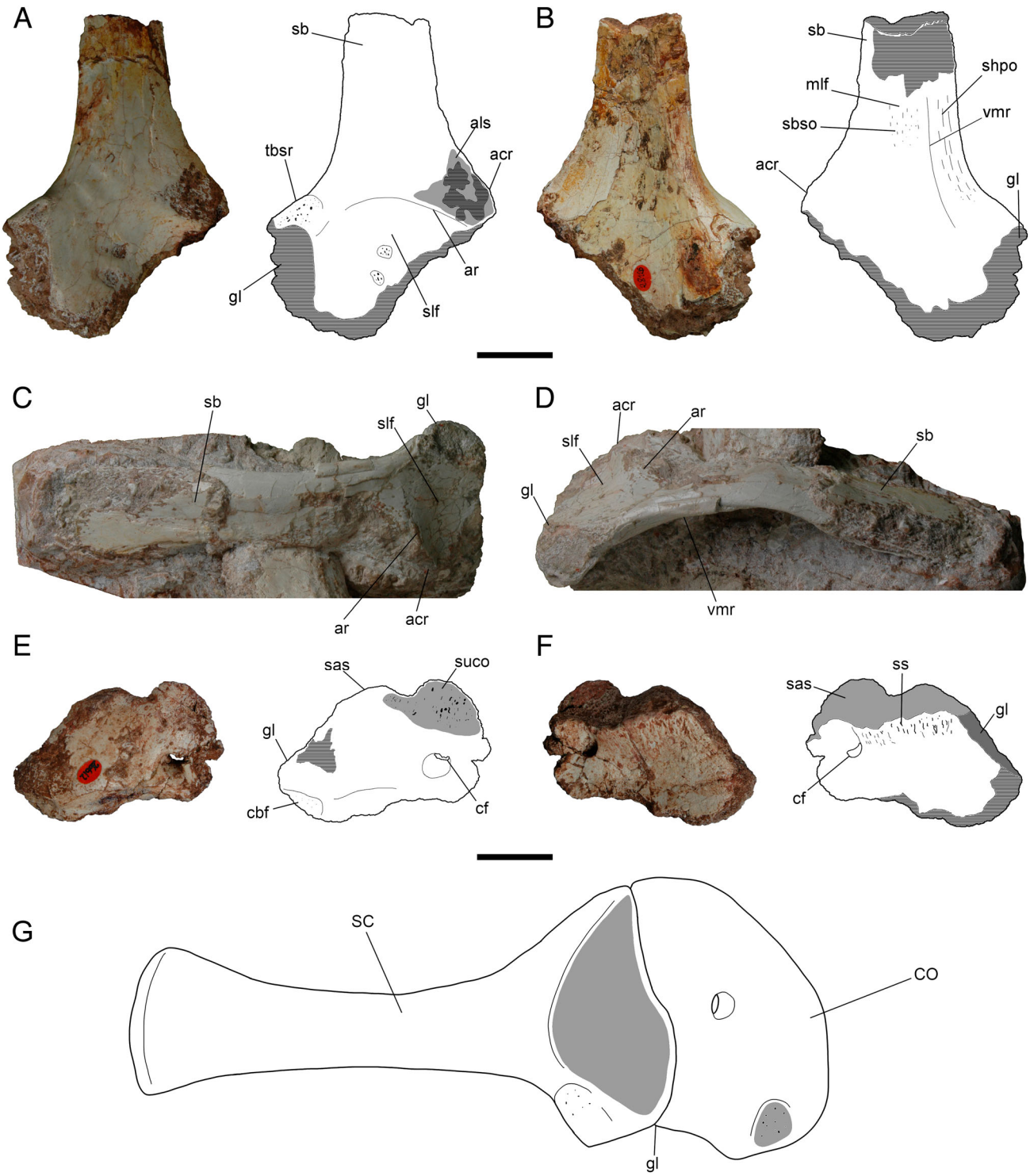

FIGURE 5. *Thecodontosaurus antiquus*, pectoral girdle. **A**, **B**, BRSUG 28126, anterior end of right scapula in **A**, lateral and **B**, medial views. **C**, **D**, BRSUG 29372-3349, left scapula in **C**, lateral and **D**, ventrolateral views. **E**, **F**, BRSUG 26612, right coracoid in **E**, lateral and **F**, medial views. **G**, reconstruction of the right scapulocoracoid complex in lateral view, based on several specimens. **Abbreviations**: **acr**, acromion; **als**, acromial lateral scar; **ar**, acromial ridge; **cbf**, M. coracobrachialis (mCB) fossa; **cf**, coracoid foramen; **CO**, coracoid; **gl**, glenoid; **mlf**, medial longitudinal fossa; **sas**, scapular articular surface; **sb**, scapular blade; **sbso**, M. subscapularis (mSBS) origin; **SC**, scapula; **shpo**, M. scapulohumeralis posterior (mSHP) origin; **slf**, scapular lateral fossa; **ss**, synchondrosis strations; **suco**, M. supracoracoideus (mSUC) origin; **slf**, scapular lateral fossa; **tbsr**, M. triceps brachii caput scapulare (mTBS) rugosity; **vmr**, ventromedial ridge. Scale bars equal 2 cm.

is very robust, as with the scapular glenoid compared with the rest of the bone, which is plate-like. In ventral view, the glenoid surface has a subrectangular shape, with its posterior end mediolaterally wider than the anterior. The coracoid foramen is large and perforates the bone in a posteromedial direction (Fig. 5E, F). The lateral opening of the foramen is wider than the medial one. An oval fossa bounded by a dorsal ridge is present on the lateral surface of the coracoid, anterior to the glenoid, and this probably served as the insertion of M. coracobrachialis (Otero, 2018). The lateral surface of the coracoid posterodorsal to the coracoidal foramen is pitted (Fig. 5E), which might represent the ventral portion of the origin site of M. supracoracoideus. Only the ventral portion of the scapular articular surface is preserved, which is concave. The medial surface of the coracoid anterior to the scapular articulation (Fig. 5F) bears deep striations corresponding to the scapulocoracoid synchondrosis, as in *Saturnalia* (Langer et al., 2007).

Humerus—The humerus is sigmoid in lateral view, with the proximal half curving posteriorly and the distal half curving anteriorly (Fig. 6). The proximal end is rotated ca. 45° with respect to the distal end, unlike in *Saturnalia*, in which both ends are in the same plane (Langer et al., 2007). Nonetheless, this rotation might be affected by taphonomic distortion. The proximal and distal ends are mediolaterally expanded compared with the slender shaft. The proximal part of the bone is anteroposteriorly flat and plate-like. The humeral head is ellipsoid and is anteroposteriorly expanded with respect to the rest of the proximal end (Fig. 6B). The medial side of the proximal humerus mediodistal to the head presents a medial tuberosity (Fig. 6D), which is bulbous and posteriorly prominent and has a grooved surface, but its medial tip is abraded in all specimens.

The well-developed deltopectoral crest forms an approximate right angle with the rest of the proximal humerus. The deltopectoral crest extends for ca. 43° of the length of the humerus, similar to the condition in most basal sauropodomorphs (Galton, 1973; Langer, 2003; Pol et al., 2011; Sereno et al., 2013; McPhee et al., 2019), including the Durdham Down *T. antiquus* and YPM 2195 (Benton et al., 2000; Galton et al., 2007). Galton (2007) noted that the deltopectoral crest of YPM 2195 had a rounded apex at 25° of the humeral length, proposing it to be an autapomorphy of *Asylosaurus* that distinguished it from the rest of the Durdham Down humeri, although this crest is incomplete in these specimens. Similarly, in all Tytherington specimens, the top of the deltopectoral crest is weathered so its exact shape cannot be determined nor the insertion of the M. supracoracoideus identified. The anterior surface of the proximal humerus medial to the deltopectoral crest is characterized by a proximodistally elongated depression that tapers distally (Fig. 6A), which represents the biceps gutter (Langer et al., 2007). A faint ridge that runs along the lateral side of the humerus, from the base of the deltopectoral crest to the shaft, might represent an intermuscular line that delimits the origin of the M. triceps brachii caput medialis (Langer et al., 2007; Burch, 2014; Otero, 2018). The lateral side of the base of the deltopectoral crest exhibits a proximodistally elongated rugose surface for the insertion of M. latissimus dorsi, which resembles the crest seen in *Buriolestes* (Cabreira et al., 2016) and *Unaysaurus* (Leal et al., 2004). Distal to this rugosity, there is a small subcircular fossa where the M. humeroradialis originated (Fig. 6B, C), a trait shared with *Saturnalia* (Langer et al., 2007) and *Unaysaurus* (Leal et al., 2004). The posterior surface of the proximal humerus exhibits two large and shallow fossae separated by an oblique ridge.

The humeral shaft has an oval cross-section at its midpoint, with an almost flat posterior margin. The shaft is relatively short compared with the expanded ends. The distal end is robust, with a transverse width ca. 33% of the proximodistal length of the bone, similar to the condition in *Saturnalia* (Langer et al., 2007) and *Unaysaurus* (McPhee et al., 2019). In anterior view, the distal end is asymmetrical, with the medial condyle more prominent than the lateral. On the anterior surface (Fig. 6E), the cuboid fossa is a wide and deep depression located between the two distal condyles, which is morphologically elaborate, presenting an irregular outline with a bilobate proximal margin and a strongly pitted surface. The cuboid fossa is also well developed in *Saturnalia* (Langer et al., 2007) and other basal sauropodomorphs, unlike the absent or poorly developed fossa of basal saurischians such as *Herrerasaurus* (Sereno, 1994) and *Tawa* (Burch, 2014). There is no evident fossa olecrani on the posterior surface of the distal humerus between the condyles, a feature seen in other sauropodomorphs such as *Saturnalia* (Langer et al., 2007) and *Sarahsaurus* (Marsh and Rowe, 2018). Both the entepicondyle and the ectepicondyle present striations on their posterolateral surfaces, possibly associated with the origin of digital flexors and extensors, respectively (Fig. 6F–H).

Ulna—The ulna presents the plesiomorphic morphology of early sauropodomorphs, with a developed olecranon process and a bowed shaft (Fig. 7A–C). It is posteriorly convex in lateral view and slightly laterally convex in anterior view. The proximal end is twice as anteroposteriorly wide as the distal end. The proximal end is triangular in proximal view, the vertices of which are the anteromedial process anteriorly, the lateral process laterally, and the olecranon process posteriorly. The medial surface of the proximal ulna is slightly concave. The radial fossa (Fig. 7A), the lateral depression for the reception of the radius that separates the anteromedial and lateral processes, is shallow. A low subcircular tubercle is present on this fossa. Proximodistally oriented long striae on the posterior surface of the proximal ulna, including the olecranon, extend distally up to 25% of the length of the ulna (Fig. 7A, B) and represent the insertion of M. triceps brachii. The apex of the olecranon process is abraded in most of the specimens, but in those that preserve it, it is less prominent than in *Saturnalia* (Langer et al., 2007) and *Chromogisaurus* (Ezcurra, 2010) and some early saurischians such as *Eodromaeus* (Martínez et al., 2011) and *Gnathovorax* (Pacheco et al., 2019).

The shaft is elliptical in cross-section with an anteroposterior long axis. A posterolateral ridge starts from the posterior edge of the shaft and extends anterodistally on the lateral surface of the bone (Fig. 7A, B). This ridge probably represents an intermuscular line. The distal end of the ulna has an elliptical outline in distal view, with its longest axis oriented anterolaterally with respect to the proximal end. The anteromedial surface of the distal end is grooved and represents the articular surface for the distal radius.

Radius—Only two radii are known from Tytherington, of which the most complete has a strongly abraded surface, and only a few features can be identified and described. The radius is a slender element, with proximal and distal ends subequal in size (Fig. 7D–F). The shaft presents a laterally convex curvature. The distal end is mediolaterally compressed. A sculptured rugosity is present on its posterolateral side, from which a posterolateral ridge extends distally, forming an acute angle between the posteromedial and posterolateral surfaces of the proximal radius. At the midpoint of the shaft, an anteromedial protuberance appears to be present (Fig. 7F), although it could be the result of taphonomic distortion. Nonetheless, the biceps tubercle is present more proximally on the anteromedial portion of the radius of *Herrerasaurus* (Sereno, 1994). The ulnar articular surface is smooth and medially concave. The distal end is subtriangular in lateral view.

Manus—Known manual elements from Tytherington are disarticulated and comprise metacarpals I to III of both sides, a proximal manual phalanx, and two unguals (Fig. 8). Numerous phalanges are also present in the collection, but due to the disarticulation and size disparity, they are very difficult to assign to the manus or the pes and therefore are excluded from the present descriptive account.

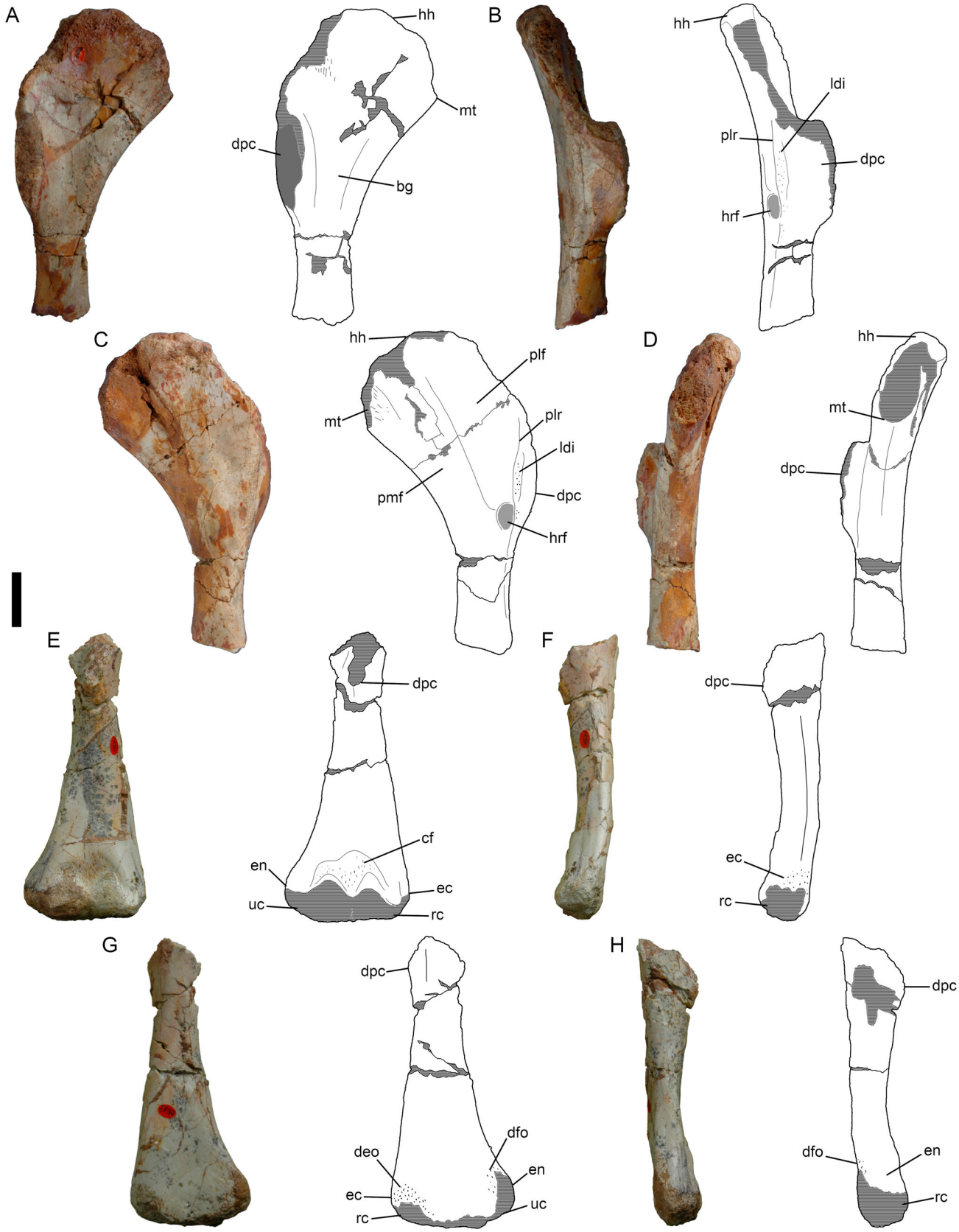

FIGURE 6. *Thecodontosaurus antiquus*, humeri. **A**–**D**, BRSUG 23608, proximal portion of right humerus in **A**, anterior, **B**, lateral, **C**, posterior, and **D**, medial views. **E**–**H**, BRSUG 28151, distal portion of left humerus in **E**, anterior, **F**, lateral, **G**, posterior, and **H**, medial views. Photographs in **B**–**D** were edited to digitally remove annotations on the fossil; see Figure S1 for the original photographs. **Abbreviations**: **bg**, biceps gutter; **cf**, cuboid fossa; **deo**, digital extensors origin; **dfo**, digital flexors origin; **dpc**, deltopectoral crest; **ec**, ectepocondyle; **en**, entepicondyle; **hh**, humeral head; **hrf**, M. humeroradialis (mHR) fossa; **ldi**, M. latissimus dorsi (mLD) insertion; **mt**, medial tuber; **pmf**, posteromedial fossa; **plf**, posterolateral fossa; **plr**, posterolateral ridge; **rc**, radial condyle; **uc**, ulnar condyle. Scale bar equals 2 cm.

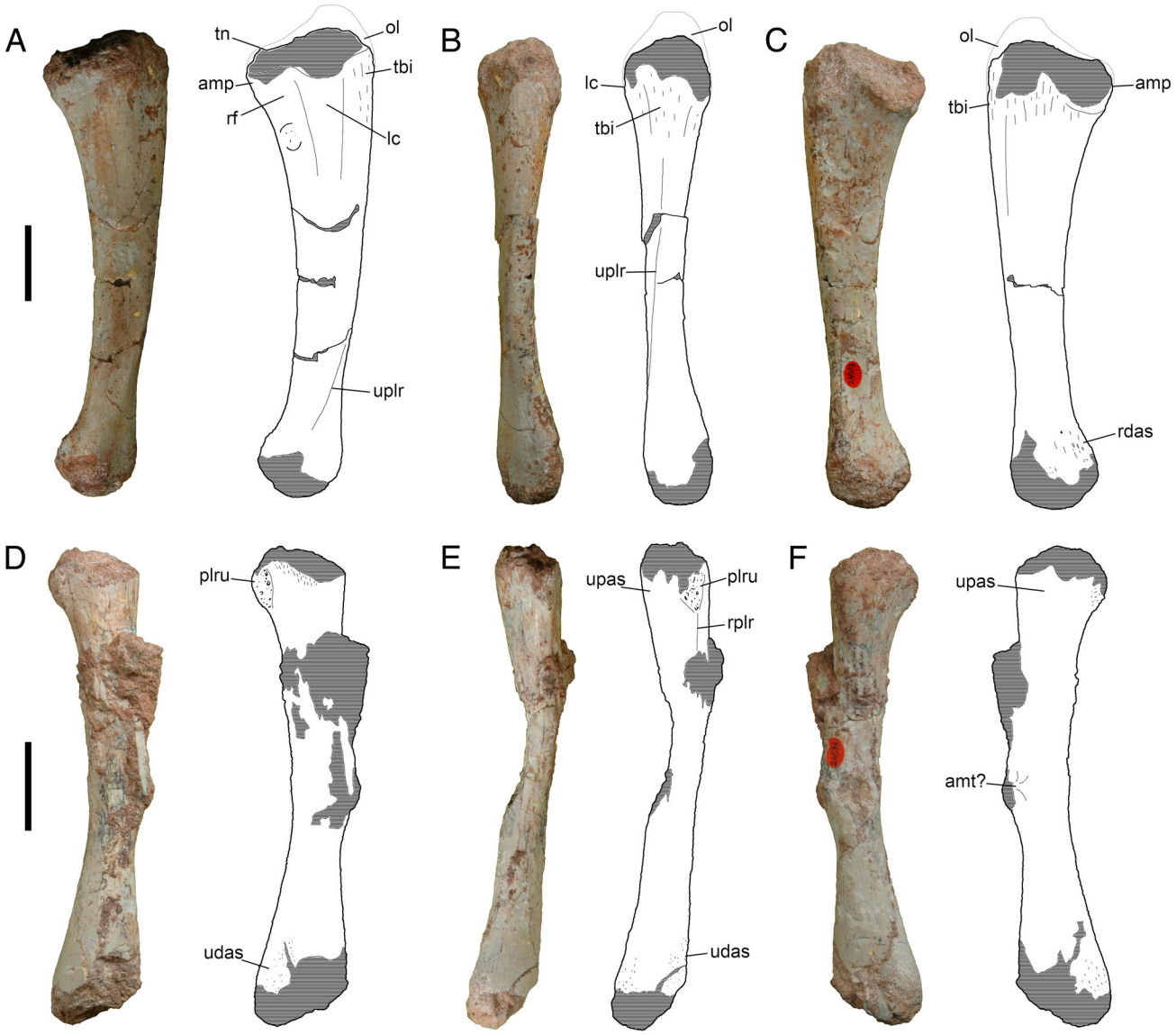

FIGURE 7. *Thecodontosaurus antiquus*, fore zeugopodium. **A**–**C**, BRSUG 26598, left ulna in **A**, lateral, **B**, posterior, and **C**, medial views. **D**–**F**, BRSUG 26594, right radius in **D**, lateral, **E**, posterior, and **F**, medial views. **Abbreviations**: **amp**, anteromedial process; **amt**, anteromedial tuberosity; **lc**, lateral condyle; **ol**, olecranon process; **plru**, posterolateral rugosity; **rdas**, distal articular surface for the radius; **rf**, radial fossa; **rplr**, posterolateral ridge of the radius; **tbi**, M. triceps brachii (mTB) insertion; **tn**, trochlear notch; **udas**, distal articular surface for the ulna; **upas**, proximal articular surface for the ulna; **uplr**, posterolateral ridge of ulna. Scale bars equal 2 cm.

Metacarpal (MC) I is the most robust metapodial element of the manus, being shorter and broader than the other metacarpals (Fig. 8A, B). The mediolateral width of the proximal end is 55% the proximodistal length of the bone, relatively broader than the MC I of *Macrocollum* (Müller et al., 2018a), but narrower than those of *Eoraptor* (Sereno et al., 2013) and more derived sauropodomorphs such as *Unaysaurus* (McPhee et al., 2019), *Adeopapposaurus* (Martínez, 2009), *Sarahsaurus* (Marsh and Rowe, 2018), or *Mussaurus* (Otero and Pol, 2013). Because manual elements are isolated, the proximal inset of MC I into the carpus, characteristic of basal sauropodomorphs (Sereno, 2007; Martínez, 2009; Otero and Pol, 2013; Sereno et al., 2013), cannot be determined. The proximal end is quadrangular in shape, with the lateral side being longer than the medial and the dorsal side longer than the palmar. The medial side is rounded in proximal view, and the lateral side is straight to slightly concave. The dorsal surface of the proximal end is pitted and rugose (Fig. 8A) and was the origin of M. extensor digitorum profundus (mEDP) on MC I. The palmar surface of the proximal end is marked by a scarred shallow concavity located on the lateral side (Fig. 8B), which represents the origin of M. flexor digitorum profundus (mFDP) on MC I (Otero, 2018). The lateral side of the proximal portion is straight to concave and directed lateropalmarly, being the articular surface for metacarpal II. The shaft is short, subequal in length to the proximal and distal ends, and dorsopalmarly compressed. A lateral depression is present immediately proximal to the lateral condyle on the dorsal surface of the shaft. The distal end is

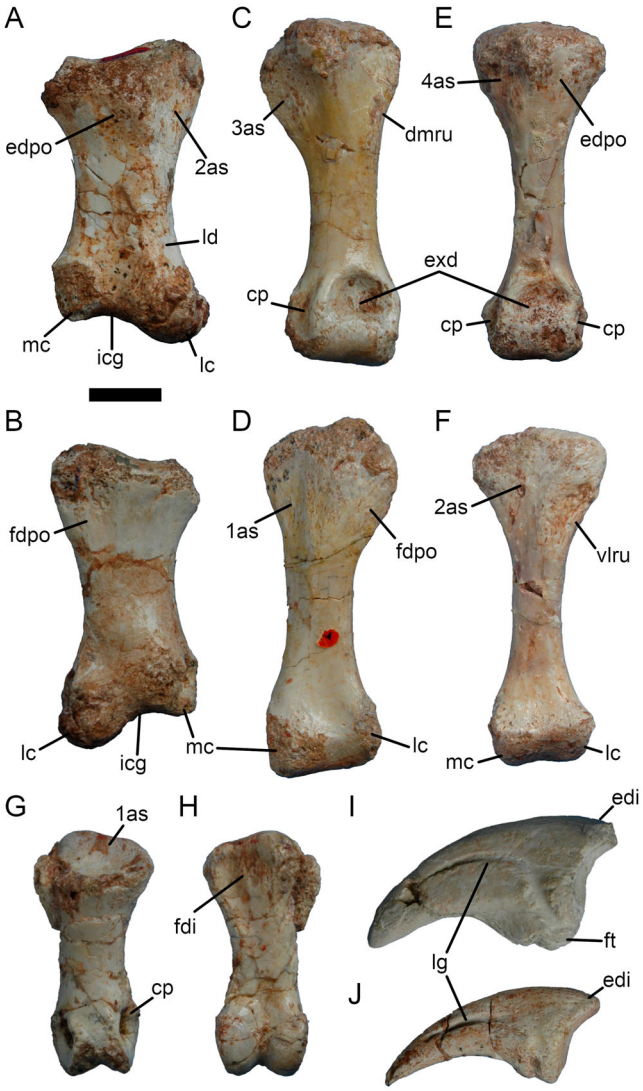

FIGURE 8. *Thecodontosaurus antiquus*, manus. **A**, **B**, BRSUG 28161, left metacarpal I in **A**, dorsal and **B**, palmar views. **C**, **D**, BRSUG 26585, right metacarpal II in **C**, dorsal and **D**, palmar views. **E**, **F**, BRSUG 29372-2828, right metacarpal III in **E**, dorsal and **F**, palmar views. **G**, **H**, BRSUG 29372-2832, proximal phalanx of manual digit I in **G**, dorsal and **H**, palmar views. **I**, BRSUG 26639, ungual phalanx of manual digit I in lateral view. **J**, BRSUG 23646, ungual phalanx of manual digit II or III in lateral view. **Abbreviations**: **1as**, metacarpal I articular surface; **2as**, metacarpal II articular surface; **3as**, metacarpal III articular surface; **4as**, metacarpal IV articular surface; **cp**, collateral pit; **dmru**, dorsomedial rugosity; **edi**, digital extensors insertion; **edpo**, M. extensor digitorum profundus (mEDP) origin; **exd**, extensor depression; **fdi**, digital flexors insertion; **fdpo**, M. flexor digitorum profundus (mFDP) origin; **ft**, flexor tubercle; **icg**, intercondylar groove; **lc**, lateral condyle; **ld**, lateral depression; **lg**, lateral groove; **mc**, medial condyle; **vlru**, ventrolateral rugosity. Scale bar equals 1 cm.

strongly asymmetrical, and hourglass-shaped in distal view, represented by two condyles separated by a deep groove. The lateral condyle is more prominent laterodistally than the medial and is more dorsopalmarly deep, particularly projecting in a dorsal direction. The medial condyle is less prominent. The lateral collateral pit is proximodistally elongated, whereas the medial pit is circular. The distal condyles are twisted ca. 15° relative to the transverse axis of the proximal end, the twist being similar to that in *Eoraptor* (Sereno et al., 2013) but less than in more derived sauropodomorphs such as *Mussaurus* (Otero and Pol, 2013).

Metacarpal II (Fig. 8C, D) is longer and narrower than MC I, but more robust than MC III. The proximal end is laterally wider than the distal end and quadrangular in proximal view. The lateral side of the proximal part of MC II is dorsolaterally oriented and concave, representing the articular surface for MC III (Fig. 8C). The medial side of the proximal portion is mediopalmarly oriented, with a shallow, heavily grooved concave surface that articulates with MC I (Fig. 8D). The palmar surfaces of the proximal portion are heavily pitted, representing the muscle scar for the origin of mFDP on MC II (Otero, 2018). The dorsomedial edge of the proximal portion presents a distally elongated rugosity extending up to the beginning of the shaft, which might represent the origin of mEDP on MC II, as well as the flat dorsal surface of the proximal end, lateral to the ridge. The shaft is straight and wider mediolaterally than dorsopalmarly, with an ellipsoid cross-section. The distal end presents dorsally a deep, subcircular extensor depression that extends up to the sides and is delimited by marked ridges on both sides. The distal end is subrectangular in distal view. The distal condyles are subequal in size and are not distally separated by an intercondylar groove. Instead, the distal surface of MC II, which articulates with the proximal phalanx of digit II, is smooth and cylindrical. The medial collateral pit is very shallow, in contrast to the deep and ovoid lateral collateral pit.

Metacarpal III (Fig. 8E, F) is more slender than the two more medial metacarpals. The proximal end is notably laterally wider than the distal end. The proximal end is relatively flat and subtriangular in proximal view, with a straight palmar side, like in *Unaysaurus* (McPhee et al., 2019). The dorsolateral side of the proximal end is slightly concave and heavily scarred, representing the articulation surface for MC IV (Fig. 8E). The palmar side of the proximal end is marked by a lateral rugose surface that represents the origin of the mFDP (Fig. 8F). The shaft is relatively longer with respect to the ends than in MC II, and it is subcylindrical. The dorsal extensor depression is shallower than in MC II, semicircular in shape due to the dorsal extension of the cylindrical phalangeal articular surface. The distal condyles are subequal in size and not separated by an intercondylar groove.

The proximal phalanx of manual digit I has an expanded proximal end and a relatively narrower distal end (Fig. 8G, H). The proximal articulation for MC I is concave and asymmetrical, divided into two facets for the distal condyles of MC I, with the lateral facet being larger than the medial one. In lateral view, the palmar margin of the proximal end extends further proximally than the dorsal margin. The shaft is circular in cross-section and subequal in length to the ends. The distal end lacks an extensor depression and presents a deep and narrow proximopalmar intercondylar groove. The distal condyles are twisted with respect to the proximal end, as seen in other basal sauropodomorphs (Martínez, 2009; Otero and Pol, 2013; Sereno et al., 2013; McPhee et al., 2019). The two well-developed circular collateral pits face mediodorsally and laterodorsally.

A number of unguals are known from Tytherington, some of them robust and dorsoventrally deep, representing manual digit I unguals (Fig. 8I). Manual ungual I is slightly mediolaterally compressed (width-to-height ratio of the proximal end of 64%), and relatively wider than in many basal sauropodomorphs (Martínez, 2009; Otero and Pol, 2013; McPhee et al., 2019). The articular surface is concave in lateral view, with a central dorsopalmar ridge that fitted to the intercondylar groove of the distal condyles of the proximal phalanx of digit I. The dorsal edge projects proximally and exhibits pits and grooves that mark the insertion of M. extensores digitorum profundus et superficialis (Otero, 2018). The palmar portion of the proximal end presents a prominent flexor tubercle with a strongly grooved surface that represents the insertion of M. flexor digitorum longus (Otero,

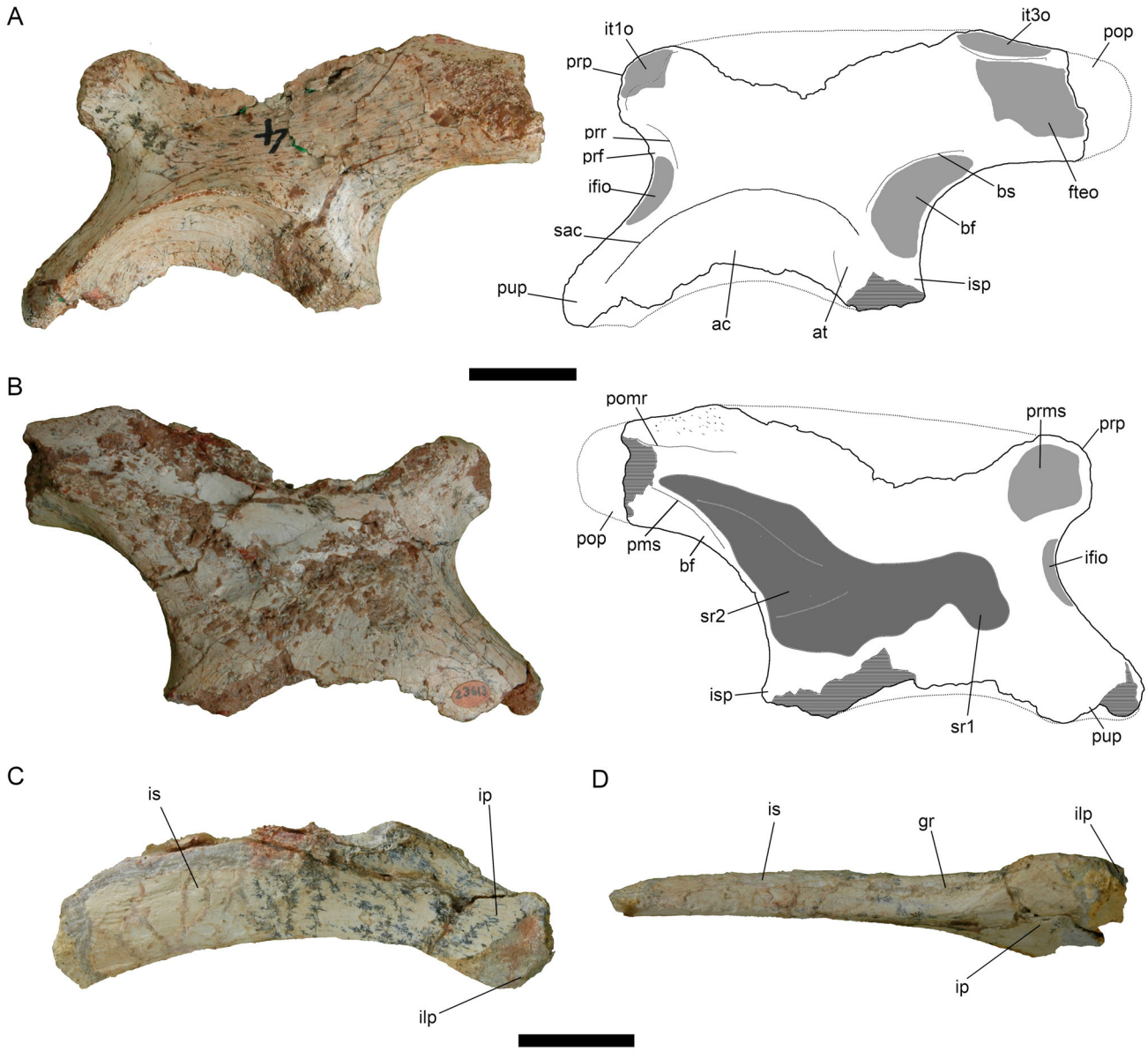

FIGURE 9. *Thecodontosaurus antiquus*, pelvic girdle. **A**, **B**, BRSUG 23613, left ilium in **A**, lateral and **B**, medial views. **C**, **D**, BRSUG 29372-3338, left ischium in **C**, lateral and **D**, posterodorsal views. **Abbreviations**: **ac**, acetabulum; **at**, antitrochanter; **bf**, brevis fossa; **bs**, brevis shelf; **fteo**, M. flexor tibialis externus (mFTE) origin; **gr**, groove; **ifio**, M. iliofemoralis internus (mIFI) origin; **ilp**, iliac peduncle; **ip**, ischiadic plate; **is**, ischiadic shaft; **isp**, ischiadic peduncle; **it1o**, M. iliotibialis 1 (mIT1) origin; **it3o**, M. iliotibialis 3 (mIT3) origin; **pms**, posteromedial shelf; **pomr**, postacetabular medial ridge; **pop**, postacetabular process; **prf**, preacetabular fossa; **prms**, preacetabular medial scar; **prp**, preacetabular process; **prr**, preacetabular ridge; **pup**, pubic peduncle; **sac**, supracetabular crest; **sr1**, first sacral rib articular surface; **sr2**, second sacral rib articular surface. Scale bars equal 2 cm.

2018). Manual ungual I is notably curved distally and presents deep collateral grooves, the proximal portions of which curve palmarly. Other ungual elements are more slender and straighter (Fig. 8J). The proximal end is dorsoventrally shorter, and the flexor tubercle is less prominent. These unguals probably belong to digits II or III, or the pes.

Ilium—Tytherington has yielded a number of *Thecodontosaurus* ilia, three of which are almost complete, enabling the accurate reconstruction of this element (Fig. 9). The ilium is anteroposteriorly longer than dorsoventrally tall, with a height-to-length (from the anterior end of the pubic peduncle to the posterior end of the postacetabular process) ratio of 54%, similar to that of *Panphagia* (52%; Martínez and Alcober, 2009) and proportionally more elongated than those of *Chromogisaurus* (61%; Ezcurra, 2010), *Saturnalia* (62%; Langer, 2003), and particularly *Buriolestes* (67%; Cabreira et al., 2016) and *Pantydraco* (68%; Galton et al., 2007; Galton and Kermack, 2010). The dorsal outline, complete in BRSUG 28121, is almost straight in lateral view.

The preacetabular process is short, with a rounded anterior outline, and is slightly curved laterally, as in the Durdham Down *T. antiquus* (NHMUK PV R1539; Benton et al., 2000). The ventral deflection of this process, used to differentiate *T. antiquuus* from *Pantydraco* (Yates, 2003a), is absent in all the Tytherington specimens and in the specimen NHMUK PV R1539 from Durdham Down (Benton et al., 2000). In anterior

view, the preacetabular process is dorsolaterally convex. The anterodorsal border of the preacetabular process shows a pitted and grooved surface (Fig. 9A) and corresponds to the insertion of M. iliotibialis 1 (Hutchinson, 2001a). The anterior margin of the ilium between the preacetabular process and the base of the pubic peduncle is anteriorly concave and 'U'-shaped in lateral view. In this part of the bone, the preacetabular fossa is present and separated from the main lateral body of the ilium by the preacetabular ridge (Fig. 9A). This fossa has a pitted surface that represents the origin of the M. iliofemoralis internus (Hutchinson, 2001a). The medial side of the preacetabular process exhibits a faintly scarred surface, similar to the condition in *Pampadromaeus* (Langer et al., 2019), which could indicate the incorporation of a dorsal vertebra into the sacrum, as seen in *Eoraptor* (Sereno et al., 2013) and sauropodomorphs more derived than *Thecodontosaurus* (Yates, 2003b).

The ilium bears a laterally prominent, dorsally convex supracetabular crest that almost reaches the ventral end of the pubic peduncle (Fig. 9A). This crest is similarly expanded in other basal sauropodomorphs (Langer, 2003; Martínez and Alcober, 2009; Ezcurra, 2010; Sereno et al., 2013; Cabreira et al., 2016; Langer et al., 2019), becomes less prominent in plateosaurians (Martínez, 2009; Apaldetti et al., 2013; Otero and Pol, 2013; McPhee et al., 2015; Marsh and Rowe, 2018, Tsai et al., 2018), and is greatly reduced in *Lessemsaurus* and eusauropods (Pol and Powell, 2007). The pubic peduncle is longer than the ischial peduncle and projects anteroventrally. The ischial peduncle is oriented ventrally and presents a slightly convex antitrochanter on its anterolateral surface, within the acetabulum. Both peduncles are subtriangular in cross-section defined by the laterally projecting supracetabular crest and a straight medial side. The acetabulum is not fully perforated, with a medial wall that extends ventrally to the level of the pubic and ischial peduncles, the plesiomorphic condition also seen in other basal sauropodomorphs (Langer, 2003; Ezcurra, 2010; Galton and Kermack, 2010; Müller et al., 2018c; Langer et al., 2019; Pretto et al., 2019) and differing from the fully perforated acetabulum of *Efraasia* and more derived sauropodomorphs (Yates, 2007; Martínez, 2009; Otero and Pol, 2013; McPhee et al., 2014; Tsai et al., 2018). The medial side of the ilium bears a sinusoidal scar that is related to the sacral rib articulations (Fig. 9B). The articular facet for the first sacral rib is subhorizontal, whereas the second sacral rib articulation is posterodorsally oriented.

The postacetabular process is more prominent than the preacetabular one, extending well posteriorly behind the ischial peduncle. It becomes mediolaterally broader posteriorly, with a robust posterior end. The process is oriented posteriorly, similar to those of *Saturnalia* (Langer, 2003), *Pampadromaeus* (Langer et al., 2019), and *Macrocollum* (Müller et al., 2018a), and unlike the posterodorsally projecting process of *Buriolestes* (Müller et al., 2018c), *Bagualosaurus* (Pretto et al., 2019), and *Pantydraco* (Yates, 2003a; Galton and Kermack, 2010). The postacetabular process presents a well-developed dorsal ridge that delimits an anteroposteriorly elongated dorsal concavity with a grooved surface (Fig. 9A) that marks the origin of M. iliotibialis 3. The posterolateral surface of the postacetabular process, ventral to the dorsal ridge, bears an extensive muscle scar for the origin of M. flexor tibialis externus, also present in *Saturnalia* (Langer, 2003), *Chromogisaurus* (Ezcurra, 2010), and *Buriolestes* (Müller et al., 2018c) and previously considered an apomorphy of Saturnaliinae (Garcia et al., 2019). On the posterior part of the ilium, ventral to the postacetabular process, a shallow brevis fossa is present, anterodorsally bounded by a faintly defined the brevis shelf in lateral view (Fig. 9A). This reduced brevis fossa is similar to that of *Pantydraco* (Yates, 2003a; Galton and Kermack, 2010) and more derived sauropodomorphs (McPhee et al., 2015; McPhee and Choiniere, 2016) and differs from the well-developed fossae of other basal sauropodomorphs (Galton, 1973; Langer, 2003; Martínez and Alcober, 2009; Ezcurra, 2010; Sereno et al., 2013; Cabreira et al., 2016). The brevis shelf is also more conspicuous in other taxa such as *Buriolestes* (Cabreira et al., 2016), *Chromogisaurus* (Ezcurra, 2010), *Pampadromaeus* (Langer et al., 2019), and *Efraasia* (Galton, 1973). The brevis fossa has a pitted surface with a different texture from the rest of the bone, marking the origin of the M. caudofemoralis brevis. In medial view (Fig. 9B), the brevis fossa is anterodorsally separated from the sacral rib articular surface by the posteromedial shelf, a feature that is also present in *Pampadromaeus* (Langer et al., 2019). Dorsal to this shelf, a dorsomedial ridge bounds a dorsomedial pitted concavity.

Ischium—Only two fragmentary ischia have been recovered from Tytherington. The distal end, the anterior edge of the shaft and the medioventral lamina are missing in the two specimens, providing an incomplete idea of this element. The ischial shaft is subrectangular in cross-section, flat, and is slightly laterally convex (Fig. 9C). The posterodorsal surface of the ischial shaft ventral to the iliac peduncle bears a groove delimited by a marked ridge on both sides that represents the origin site for M. adductor femoris 2 (Hutchinson, 2001a).

Femur—Several femora attributable to *Thecodontosaurus* were found at Tytherington, some of them almost complete (Fig. 10). There is a remarkable variation in size among Tytherington femora, with the complete specimens ranging 12–22 cm in length (Fig. S2).

The femur is sigmoid in anterior view, with an anteromedially projecting head and a posterior end that is curved in a posterolateral direction (Fig. 10). In dorsal view, the main axes of the femoral head and the distal end form an angle greater than 90°. The proximal end of the femur is abraded in most specimens; consequently, the morphology of the greater trochanter cannot be determined. The femoral head has a semicircular shape, with flat anterior and posterior sides. Its medial orientation delimits a medially concave ventral emargination distal to it. Distal to this emargination, a large oval foramen for the femoral nutrient artery is present on the medial surface of the bone (Fig. 10D). The proximal end of the femur has a reduced anterolateral tuber that is connected to the proximal tip of the lesser trochanter by an oblique anteromedial crest, as seen in other basal sauropodomorphs (Langer, 2003; Müller et al., 2018a, 2018c; Langer et al., 2019). A faint posteromedial tuber is also present at the proximal end, shared by other basal taxa (Langer, 2003; Müller et al., 2018c; Langer et al., 2019) and less developed than in *Macrocollum* (Müller et al., 2018a).

A synapomorphic feature of the proximal femur of *Thecodontosaurus* is the absence of a trochanteric shelf (Fig. 10A). This structure evolved in Dinosauriformes (Novas, 1996) and is retained by other basal sauropodomorphs such as *Buriolestes* (Müller et al., 2018c), *Pampadromaeus* (Langer et al., 2019), and *Bagualosaurus* (Pretto et al., 2019), but lost in more derived sauropodomorphs (Galton, 1973; Martínez, 2009; Müller et al., 2018a; Barrett et al., 2019). This character seems to be affected by ontogeny in *Pampadromaeus*, because juvenile specimens lack a trochanteric shelf, which is seen in adults (Müller et al., 2019), although this is probably not the case in *Thecodontosaurus* because this structure is absent in juvenile to adult femora (Fig. S2). This indicates that *Thecodontosaurus* is among the most basal taxa to lose the trochanteric shelf. The lesser (anterior) trochanter is proximodistally elongated and located on the anterolateral surface of the proximal femur. The proximal tip of the lesser trochanter is completely attached to the shaft, as in *Pampadromaeus* (Müller et al., 2015; Langer et al., 2019) and unlike in *Saturnalia*, in which it is separated by a cleft (Langer and Ferigolo, 2013). A shallow fossa proximolaterally bounds the lesser trochanter and in turn is laterally delimited by the rugose dorsolateral trochanter (Fig. 10A, B). Both the lesser trochanter and the fossa present a pitted and grooved

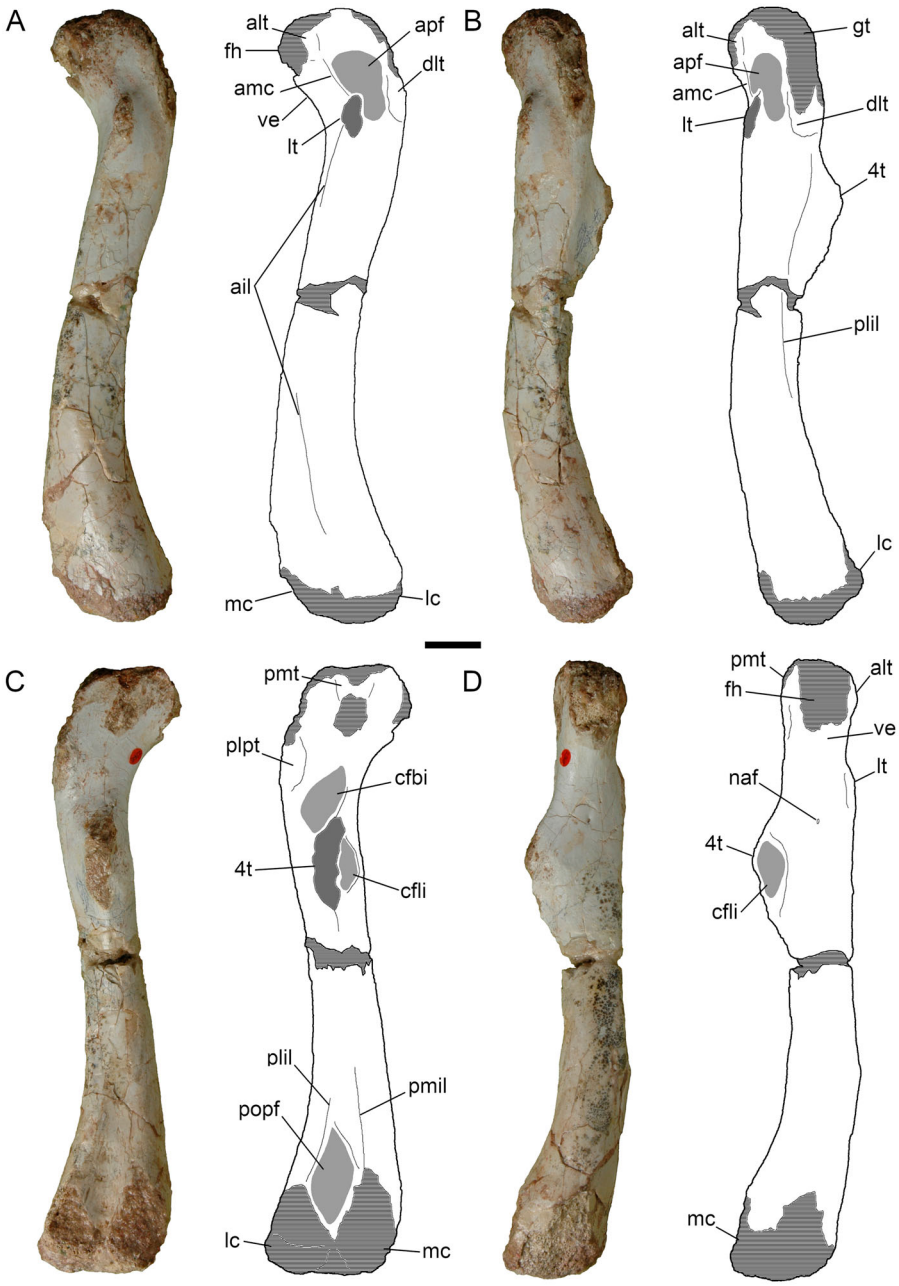

FIGURE 10. *Thecodontosaurus antiquus*, BRSUG 23615, left femur in **A**, anterior, **B**, lateral, **C**, posterior, and **D**, medial views. **Abbreviations**: **4t**, fourth trochanter; **ail**, cranial intermuscular line; **alt**, anterolateral tuber; **amc**, anteromedial crest; **apf**, anterior proximal fossa; **cfbi**, M. caudofemoralis brevis (mCFB) insertion; **cfli**, M. caudofemoralis longus (mCFL) insertion; **dlt**, dorsolateral trochanter; **gt**, greater trochanter; **fh**, femoral head; **lc**, lateral condyle; **lt**, lesser trochanter; **mc**, medial condyle; **naf**, nutrient artery foramen; **plil**, caudolateral intermuscular line; **plpt**, posterolateral proximal tuberosity; **pmil**, caudomedial intermuscular line; **pmt**, posteromedial tuber; **popf**, popliteal fossa; **ve**, ventral emargination. Scale bar equals 2 cm.

surface that represents the muscle scar for the insertion of M. iliofemoralis (Hutchinson, 2001b). A dorsolateral trochanter located on the anterolateral proximal femur laterally delimits this fossa and would have been continuous with the greater trochanter. On the posterolateral surface of the proximal femur, a similar rugose and pitted feature, the posterolateral proximal tuberosity, is present (Fig. 10C).

In BRSUG 23615, the shaft has a diameter of 2.1 cm at its midpoint, with a diameter-to-length ratio of 10%. The shaft is subtriangular in cross-section due to the presence of three intermuscular lines. The anterior intermuscular line runs from the distal end of the lesser trochanter to the anterior surface of the lateral distal condyle (Fig. 10A). The posteromedial intermuscular line is continuous with the distal end of the fourth trochanter and ends at the medial condyle (Fig. 10C). The third intermuscular line, the posterolateral one, has its origin distal to the greater trochanter and reaches the posterior surface of the lateral condyle (Fig. 10B). The anterior and posteromedial intermuscular lines delimit the origin site of M. femorotibialis medialis, and the anterior and posterolateral lines bound that of M. femorotibialis lateralis (Hutchinson, 2001b).

The fourth trochanter is subrectangular and placed on the posterior part of the femur, with its distal tip located ca. 40% along the bone in BRSUG 23615. The fourth trochanter is also located in the proximal half of the femur in other basal sauropodomorphs (Galton, 1973; Otero and Pol, 2013; Cabreira et al., 2016; Müller et al., 2018b) and becomes more distally positioned in *Melanorosaurus*, *Anchisaurus*, *Aardonyx*, and more derived sauropodiforms (Yates and Kitching, 2003; Galton et al., 2005; Yates et al., 2010). The medial surface of the trochanter bears a

clear concave muscle scar with a highly pitted surface that represents the insertion of M. caudofemoralis longus (Fig. 10C, D). The proximolateral portion of the fourth trochanter exhibits a teardrop-shaped pitted surface and was the insertion of M. caudofemoralis brevis (Fig. 10C). Variation in fourth trochanter morphology and position associated with size can be described among the different *Thecodontosaurus* femora from Tytherington (Fig. S2). This structure seems to experience negative allometry throughout ontogeny, because its proximodistal length is relatively greater (20% of total femoral length) in BRSUG 26602, a possible hatchling specimen of 12 cm in length, compared with larger femora (16% in BRSUG 23615, of 22 cm). Additionally, the relative position of the fourth trochanter seems to shift proximally with size: the distal end of the trochanter is located at 44% of the femoral length in BRSUG 26602 and at 40% in BRSUG 23615. These changes possibly had implications for locomotion throughout ontogeny, particularly affecting the orientation and moment arms of the caudofemoralis musculature.

The distal condyles are slightly asymmetrical, with the lateral (fibular) condyle being more prominent as a result of the slight lateral curvature of the distal end of the femur (Fig. 10C). In posterior view, the condyles are laterally pinched and separated by the popliteal fossa, a marked concavity with extensive pitting, bounded by the distal segments of the posteromedial and posterolateral intermuscular lines (Fig. 10C). In some specimens (e.g., BRSUG 29372-2882), a muscle scar is seen on the lateral surface of the distal femur, anteroproximal to the fibular condyle. This scar might be homologous to the anteromedial distal crest of other dinosaurs (Hutchinson, 2001b), an osteological correlate for the attachment of the distal head of M. femorotibialis lateralis. Further evidence of muscle scarring is found on the anterolateral surface of the distal end of the femur, proximal to the lateral condyle, probably representing the femoral origin of the digital extensors. The distal surface of the femur is abraded in all specimens, making the interpretation of features on the zeugopod articular surface complicated.

Tibia—Tibial morphology is reconstructed based on several specimens of different sizes, bracketed between the smallest (13.3 cm), possibly a juvenile, and the largest (19.7 cm). The tibia is a straight bone with anteroposteriorly expanded ends, the proximal end being twice as anteroposteriorly wide as the distal (Fig. 11A, B). The proximal end is subtriangular in proximal view, with the three edges represented by the anterior cnemial crest and the medial and lateral condyles (Fig. 11C). The cnemial crest is anteroproximally projected and extends about a fourth of the length of the tibia. The surface of the crest is pitted, marking the insertion scar of the muscles that form the triceps femoris group. The cnemial crest and the lateral condyle are separated by a shallow anterolateral notch, the incisura tibialis (Fig. 11A). Anterodistal to the lateral condyle, an oval rugosity with a pitted surface is present in some specimens, such as BRSUG 26656. This structure is also present in *Saturnalia* (Langer, 2003) and is homologous to the fibular crest of *Eoraptor* and some theropods (Sereno et al., 2013). Such a rugosity serves for articulation with the fibula and the insertion of the tibiofibularis ligament (Langer, 2003). The lateral condyle does not extend posteriorly as far as the medial one, being placed at the middle of the proximal tibia in lateral view. The medial and posterior surfaces of the medial condyle present a pitted and grooved pattern indicative of muscle attachment (Fig. 11B), possibly for the insertion of M. flexor tibialis internus and M. flexor tibialis externus, components of the flexor cruris group.

The shaft is straight and subrectangular in cross-section, with flattened medial and lateral sides and an anteroposterior axis slightly longer than the mediolateral axis. On the lateral surface of the proximal fourth of the tibia, a large, oval nutrient foramen for the passage of the tibialis cranialis artery is present in BRSUG 26656, as seen in *Saturnalia* (Langer, 2003). The distal end of the tibia in *Thecodontosaurus* exhibits a highly derived morphology, being slightly wider mediolaterally than anteroposteriorly and with an almost squared outline in distal view. The anterior portion of the distal end consists of an anterolateral process that distally bears a concave facet for the astragalar ascending process (Fig. 11D). This facet is posteriorly bounded by a convex posterolateral descending process, anteroposteriorly wider than in other basal sauropodomorphs such as *Eoraptor* (Sereno et al., 2013), *Saturnalia* (Langer, 2003), *Panphagia* (Martínez and Alcober, 2009), *Adeopapposaurus* (Martínez, 2009), *Coloradisaurus* (Apaldetti et al., 2013), and *Mussaurus* (Otero and Pol, 2013). However, the posterolateral process is mediolaterally compressed and does not extend as far laterally as the anterolateral process, which is a proposed synapomophy of Sauropoda (Yates, 2004; Pol and Powell, 2007; Yates and Kitching, 2003; Ezcurra and Apaldetti, 2012; McPhee et al., 2014), also present in *Anchisaurus polyzelus* (Yates, 2004), *Eucnemesaurus entaxonis* (McPhee et al., 2015), and *Aardonyx* (Yates et al., 2010). A proximodistally oriented notch runs along the lateral surface of the distal end of the tibia and separates the anterolateral and posterolateral processes. This notch is remarkably reduced compared with other basal sauropodomorphs (Langer, 2003; Martínez, 2009; Martínez and Alcober, 2009; Apaldetti et al., 2013; Otero and Pol, 2013; Sereno et al., 2013) and resembles that in PULR 136 and *Antetonitrus* (Yates and Kitching, 2010; Ezcurra and Apaldetti, 2012; McPhee et al., 2014). Unlike in *Riojasaurus* and PULR 136, a notch is absent from the posteromedial corner of the distal end of the tibia (Ezcurra and Apaldetti, 2012).

Fibula—No complete fibula is preserved, but some partial specimens have been found at Tytherington. The fibula is a slender and straight bone. The proximal end is rounded in lateral view and anteroposteriorly elongated and mediolaterally compressed, with an oval proximal head in proximal view. The head is heavily scarred, indicating that it was covered by a cartilaginous sheath (Fig. 11F). Within the proximal part of the bone, there is a proximodistally elongated anterolateral tubercle that bears scarring and was the insertion of M. iliofibularis (Fig. 11E). On the medial side and slightly distal to this scar, a medial pitted ridge is present (Fig. 11F), which is less pronounced and proximodistally elongated than that in *Buriolestes* (Müller et al., 2018c) and *Gnathovorax* (Pacheco et al., 2019). The distal end of the fibula is anteroposteriorly expanded and oval in distal view. The distal surface is proximomedially oriented and anterodistally inclined. The medial surface of the distal end is slightly expanded and presents an ornamented articular facet for the astragalus.

Pes—Disarticulated elements of the pes have been found at Tytherington, including metatarsals I to IV of both sides and some proximal and possible distal pedal phalanges (Fig. 12).

The orientation of metatarsal (MT) I differs from that of the other elements of the metatarsus, as indicated by the articular surface for MT II, facing more medially than the other pedal metapodials. The shape of MT I (Fig. 12A–D) indicates that it was appressed to MT II, with its distal end not notably separated from the latter. The proximal and distal ends are subequal in size (Fig. 12A–D), and they are not rotated relative to each other, unlike in other sauropodomorphs such as *Pampadromaeus* (Langer et al., 2019) or *Adeopapposaurus* (Martínez, 2009). The proximal end and the shaft are mediolaterally compressed. The elliptical proximal end presents a rugose lateroplantar side that articulates with MT II (Fig. 12B). The maximum width of the proximal end is 34% the proximodistal length of the bone, being proportionally more robust than in Carnian sauropodomorphs (Sereno et al., 2013; Langer et al., 2019; Pretto et al., 2019), but within the range of most post-Carnian basal sauropodomorphs such as *Adeopapposaurus* (Martínez, 2009), *Coloradisaurus* (Apaldetti et al., 2013), *Leonerasaurus* (Pol et al., 2011),

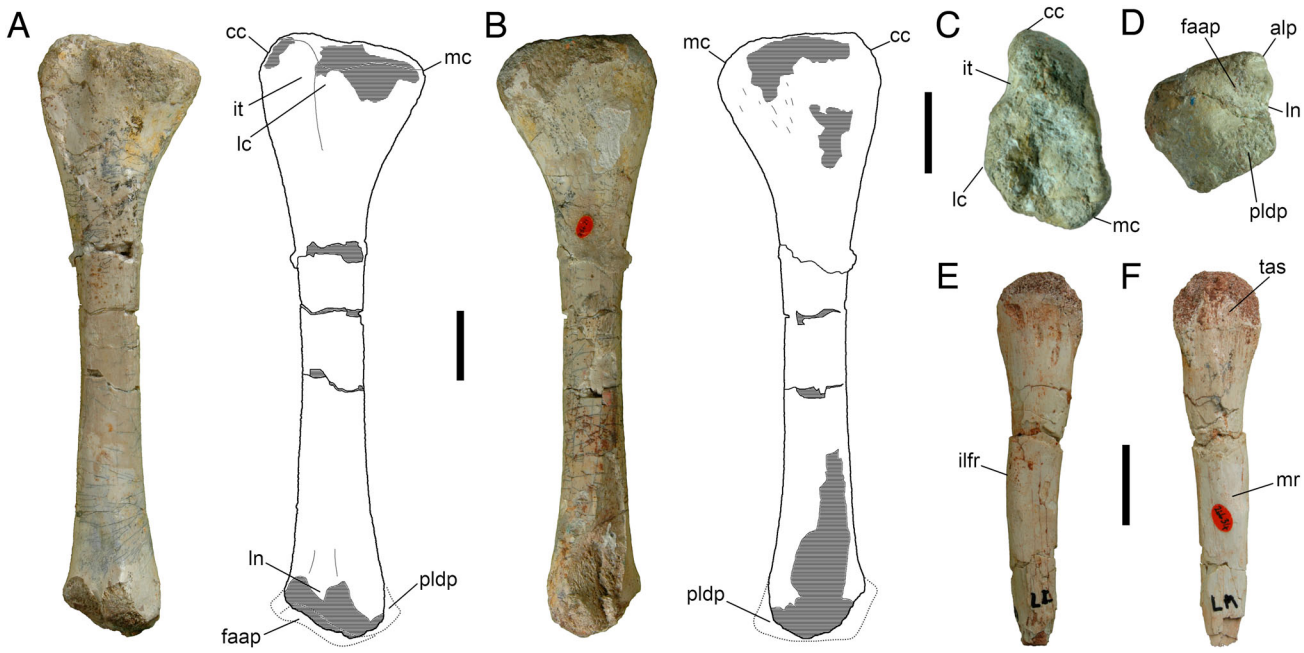

FIGURE 11. *Thecodontosaurus antiquus*, hind zeugopodium. **A**–**C**, BRSUG 23621, left tibia in **A**, lateral, **B**, medial, and **C**, proximal views. **D**, BRSUG 23647, left tibia in distal view. **E**, **F**, BRSUG 26634, proximal portion of left fibula in **E**, lateral and **F**, medial views. **Abbreviations**: **alp**, anterolateral process; **cc**, cnemial crest; **faap**, articular facet for the astragalar ascending process; **ilfr**, M. iliofibularis (mILFB) rugosity; **it**, incisura tibialis; **lc**, lateral condyle; **ln**, lateral notch; **mc**, medial condyle; **mr**, medial ridge; **pldp**, posterolateral descending process; **tas**, tibial articular surface. Scale bars equal 2 cm.

Sarahsaurus (Marsh and Rowe, 2018), and *Mussaurus* (Otero and Pol, 2013). The minimum transverse width of the shaft is 19% of the MT I proximodistal length, which is slightly lower than in most post-Carnian basal sauropodomorphs (McPhee et al., 2014, 2019), but higher than in Carnian sauropodomorphs (Sereno et al., 2013; Langer et al., 2019; Pretto et al., 2019). The orientation of MT I results in the extensor depression facing dorsomedially and the collateral pits facing dorsally and plantarly. The extensor depression is deep and subcircular in outline, and it is distally bounded by a prominent ventromedially facing phalangeal articular surface that lacks an intercondylar groove (Fig. 12B). The distal condyles differ in size, with the dorsolateral one being bigger and more prominent. No clear muscle scars are present in MT I, as in *Saturnalia* (Langer, 2003) and unlike in *Herrerasaurus* (Novas, 1994).

Metatarsal II (Fig. 12E–H) is long and one of the weight-bearing elements of the metatarsus, unlike MT I. The proximal end is flat and rectangular in proximal view, dorsoplantarly expanded and mediolaterally compressed, as in *Saturnalia* (Langer, 2003) and *Herrerasaurus* (Novas, 1994) and unlike the hourglass shape in more derived sauropodomorphs (Martínez, 2009; Otero and Pol, 2013). The dorsal (anterior) surface of the proximal end is concave and grooved (Fig. 12E), probably indicating the insertion of M. tibialis anterior (Carrano and Hutchinson, 2002), as in other metatarsals. Its mediodorsal side is concave and contacted the proximal end of MT I, whereas the lateroplantar side is flat and contacted MT III (Fig. 12F). The long axis of the proximal end is rotated ca. 60° with respect to the transverse axis of the distal end (Fig. 12G, H), as in *Mussaurus* (Otero and Pol, 2013). The shaft is long and straight, with a subcircular cross-section. The distal end is slightly medially curved, with distal condyles that are subequal in size and separated by a shallow intercondylar groove that continues posteriorly. The dorsal extensor depression is shallow and semicircular in shape. The lateral collateral pit is deep, whereas the medial one is absent.

Metatarsal III (Fig. 12I–L) is a long and slender weight-bearing element. In proximal view, the proximal end is subtriangular with a rounded plantar border. The dorsomedial surface of the proximal MT III is flat and contacts MT II (Fig. 12I). The lateroplantar side of the proximal end is concave and houses the medial projection of proximal MT IV (Fig. 12J). The long axes of both ends are twisted ca. 45° from one another (Fig. 12K, L). On the dorsolateral edge of the proximal shaft, a pitted proximodistally elongated scar is present. The shaft is long, and its cross-section is wider mediolaterally than dorsoplantarly, with a straight dorsal margin. The distal end is medially curved as in MT II and presents a deep lateral collateral pit and a shallow medial collateral depression. The dorsal extensor depression is shallow and semicircular.

Metatarsal IV (Fig. 12M–P) is the third weight-bearing element of the metatarsus. It is proportionately more robust than MT III. The proximal end is remarkably wide mediolaterally and flattened dorsoplantarly. The outline of the proximal end is subtriangular, with a straight plantar side and an obtuse angle formed by the dorsal and dorsomedial sides. The proximal surface of MT IV is concave, with a marked depression at the center, probably for the reception of distal tarsal IV. The dorsomedial side of proximal MT IV projects medially to contact MT III plantarly (Fig. 12M). A proximodistally elongated crest is present on the dorsal surface distal to the MT III articular surface. The plantar surface of proximal MT IV shows an oval medial rugosity and a reduced articular surface for MT V on the lateral corner (Fig. 12N). The shaft is mediolaterally wider than dorsoplantarly and is slightly sigmoid in lateral view. Unlike in other metatarsals, the distal end presents similar dorsoplantar and mediolateral lengths, whereas in *Saturnalia* it is not subequal (Langer, 2003). The distal condyles are not separated by an intercondylar groove. There is no

FIGURE 12. *Thecodontosaurus antiquus*, pes. **A**–**D**, BRSUG 26606, left metatarsal I in **A**, dorsal, **B**, plantar, **C**, proximal, and **D**, distal views. **E**–**H**, BRSUG 26627, right metatarsal II in **E**, dorsal, **F**, plantar, **G**, proximal, and **H**, distal views. **I**–**L**, BRSUG 23627, left metatarsal III in **I**, dorsal, **J**, plantar, **K**, proximal, and **L**, distal views. **M**–**P**, BRSUG 29372-3812, right metatarsal IV in **M**, dorsal, **N**, plantar, **O**, proximal, and **P**, distal views. **Q**, **R**, BRSUG 28218, proximal phalanx of pedal digit III in **Q**, dorsal and **R**, plantar views. **S**, **T**, BRSUG 29372-2851, proximal phalanx of pedal digit IV in **S**, dorsal and **T**, plantar views. **U**, BRSUG 29372-2839, distal pedal phalanx in dorsal view. **V**, BRSUG 29372-2840, distal pedal phalanx in dorsal view. **C**, **G**, **K**, **O**, dorsal toward the bottom; **D**, **H**, **L**, **P**, dorsal toward the top. **Abbreviations**: **1as**, metatarsal I articular surface; **2as**, metatarsal II articular surface; **3as**, metatarsal III articular surface; **4as**, metatarsal IV articular surface; **5as**, metatarsal V articular surface; **cp**, collateral pit; **dls**, dorsolateral scar; **exd**, extensor depression; **lc**, lateral condyle; **mc**, medial condyle; **mdru**, mediodorsal rugosity; **mpru**, medioplantar rugosity; **tai**, M. tibialis anterior (mTA) insertion. Scale bar equals 1 cm.

medial collateral pit, and the lateral collateral pit is wide, deep, and subtriangular.

Two phalanges can be identified as proximal pedal phalanges and probably belonging to digit II, III, or IV. One is more elongated and has a more slender shaft, probably belonging to digit III (Fig. 12Q, R), whereas the other is shorter and more robust and thus could be assigned to digit IV (Fig. 12S, T). They are hourglass-shaped in dorsal view, with proximal and distal ends of almost equal mediolateral widths. The proximal end is concave and semicircular in outline, with a straight plantar side and a proximally projecting dorsal margin. The proximal end is wider mediolaterally than dorsoplantarly. The collateral pits are deep, and the extensor fossa is shallow. The distal condyles are equal in size and separated by a shallow and wide intercondylar depression. Some short and robust phalanges of small size are likely distal pedal phalanges (Fig. 12U, V), but difficult to assign to specific digits.

DISCUSSION

The Taxonomic Status of *Thecodontosaurus*

The sauropodomorph material from Tytherington shares characters that support its assignment to *Thecodontosaurus antiquus*. From the original diagnosis of the species (Benton et al., 2000), the only apomorphy that can be assessed, a subquadratic posterior end of the postacetabular process of the ilium, is matched by Tytherington ilia. This character was later identified as a plesiomorphy (Yates, 2003a), although recent sauropodomorph discoveries show its variability and continuous variation (e.g., Langer, 2003; Cabreira et al., 2016; Pretto et al., 2019), making it a poor diagnostic trait. Yates (2003a) proposed an emended diagnosis of the genus *Thecodontosaurus*, of which two characters, (1) extreme posterior position of the neural spines in anterior and middle caudal vertebrae and (2) reduced ventral groove in anterior caudals and absent in middle and posterior caudals, are clearly identified in the Tytherington vertebrae (Fig. 3E–K), although a reduced ventral groove is present in Tytherington posterior caudals (Fig. 3K). However, these two traits have poor diagnostic power: the first one fails to discriminate *Thecodontosaurus* from other basal sauropodomorphs, such as *Chromogisaurus* (Ezcurra, 2010), *Bagualosaurus* (Pretto et al., 2019), or *Efraasia* (Galton, 1973), and the second character is equivocal for being highly variable at both intra- and interspecific levels (Yates, 2004; Martínez, 2009; Ezcurra, 2010; Marsh and Rowe, 2018; Langer et al., 2019). A third *Thecodontosaurus* apomorphy, anterior cervical epipophyses plate-like and overhanging the postzygapophyses posteriorly, was later considered diagnostic of *Pantydraco caducus* instead by Galton and Kermack (2010), who argued that the Durdham Down cervicals formed raised ridges. However, the Tytherington cervicals have plate-like epipophyses (Fig. 2D) that do not overhang the posterior margin of the postzygapophyses, a condition that we also identify in the Durdham Down material.

Yates (2003a) noted two additional characters of *T. antiquus* that differed from *T.* (now *Pantydraco*) *caducus*: a strongly projecting medial tuberosity of the humerus and a ventrally oriented preacetabular process of the ilium. The first of these two characters is problematic, because the tip of the humeral medial tuberosity is highly abraded in most of the *Thecodontosaurus* and *Pantydraco* specimens (Benton et al., 2000; Galton et al., 2007; Galton and Kermack, 2010), including the Tytherington humeri (Fig. 6). Only YPM 2195 seems to preserve a complete medial tuberosity, which projects strongly in a medial direction (Benton et al., 2000; Galton, 2007). Thus, this character is not valid for establishing differences between *Thecodontosaurus*, *Pantydraco*, and the problematic *Asylosaurus*. Similarly, all Tytherington ilia have an anteriorly oriented preacetabular process, as in *Pantydraco* and unlike the interpretation of the Durdham Down ilia (Yates, 2003a; Galton and Kermack, 2010). The orientation of this process, as well as a few other iliac traits, has been reported to be affected by taphonomic deformation in other basal sauropodomorphs because of its fragility (Müller et al., 2018b). Although the morphology of the preacetabular process, as well as other iliac characters, is different in *T. antiquus* and *P. caducus*, its orientation results in confusion when used to diagnose taxa. Therefore, we consider these two characters ineffective in distinguishing *T. antiquus* from *P. caducus*.

The diagnosis of *Pantydraco caducus* included the presence of pleurocoel-like openings on the neurocentral suture of the sixth to eight cervicals as an autapomorphy (Yates, 2003a; Galton and Kermack, 2010). This is the remaining character, together with the position of the anterior cervical epipophyses, that distinguished *Pantydraco* from *T. antiquus*, and it is also absent in the Tytherington cervicals. Nonetheless, this character is problematic and is affected by ontogeny, because these openings commonly occur in juvenile sauropods (Wedel, 2003, 2007). When first described, *Pantydraco* was identified as a juvenile *T. antiquus* (Kermack, 1984; Benton et al., 2000), and the differences between the two were attributed to morphological variation in ontogenetic states of the same taxon. In cladistic analyses, *Pantydraco* is consistently recovered as the sister taxon either to *Thecodontosaurus* (Bronzati et al., 2019; Langer et al., 2019; Pretto et al., 2019) or to the clade including *Thecodontosaurus* and more derived sauropodomorphs (Otero and Pol, 2013; McPhee et al., 2015), indicating that it might belong to the same taxon or that the more basal position of *Pantydraco* is because it retains some plesiomorphic character states due to its early ontogenetic stage. In conclusion, anatomical, phylogenetic, and biochronological evidence renders the validity of *Pantydraco caducus* uncertain and opens the possibility that it represents an immature individual of *T. antiquus*.

Three autapomorphies were originally proposed for *Asylosaurus yalensis* (Galton, 2007): deltopectoral crest with a round apex at 25% of the humeral length, manus with phalangeal lateral reduction (phalangeal formula 2-3-4-2-?1), and ischia distally separated by a medial cleft with an inverted 'V' shape in dorsal view. As discussed above, the first character is problematic in establishing differences from *Thecodontosaurus*, because the deltopectoral crest is not intact in any of the Durdham Down or Tytherington humeri (Benton et al., 2000; Galton et al., 2007). Additionally, the morphology of the tip of the deltopectoral crest is susceptible to taphonomic distortion (Yates, 2003a; Langer et al., 2007), so the presence of the apex in YPM 2195 could be partly caused by these processes. Second, the phalangeal formula is unknown in *Thecodontosaurus*, because a complete, articulated manus has not been found, making the second character ineffective in distinguishing YPM 2195 as a separate taxon. Additionally, lateral reduction of the manual phalangeal count is a phenomenon that also occurs in other basal sauropodomorphs such as *Eoraptor* (Sereno et al., 2013) and *Sarahsaurus* (Marsh and Rowe, 2018). The third character is based on ischium fragments that were tentatively referred to *Asylosaurus*, without any evidence (Galton, 2007). Thus, none of the three synapomorphies of *Asylosaurus* proposed by Galton (2007) provides solid diagnostic evidence for the validity of this genus. The taxonomic status of *Asylosaurus* has not been further examined because it has not been included in phylogenetic analyses as an independent taxon, but as *Thecodontosaurus* in Sertich and Loewen (2010). However, Galton and Kermack (2010) suggested that *Asylosaurus* would probably occupy a position close to *Thecodontosaurus* and *Pantydraco*. Based on the lack of diagnostic traits to distinguish it from *Thecodontosaurus*, we consider *Asylosaurus yalensis* a taxon of highly questionable validity.

Paleobiology and Ecology of *Thecodontosaurus*

Thecodontosaurus is the basal-most sauropodomorph, excluding *Pantydraco*, that lived in the Northern Hemisphere (Otero and Pol, 2013; McPhee et al., 2015; Langer et al., 2019; Pretto et al., 2019) and thus has great importance in documenting the ecological evolution of sauropodomorphs. The first sauropodomorphs from the Carnian of South America exhibited notable variation in craniodental morphology (Bronzati et al., 2019; Müller and Garcia, 2019) soon after the origin of the clade. The basal-most sauropodomorph *Buriolestes* (Cabreira et al., 2016; Müller et al., 2018c) exhibits spaced, posteriorly curved tooth crowns with fine serrations that indicate a faunivorous diet (Cabreira et al., 2016; Bronzati et al., 2019; Müller and Garcia, 2019). Other contemporary taxa such as *Eoraptor* and *Saturnalia* have some ambiguous craniodental traits, but which are consistent with predominantly carnivorous habits (Sereno et al., 2013; Bronzati et al., 2017, 2019; Müller and Garcia, 2019). Three genera of Carnian sauropodomorphs (*Panphagia*, *Pampadromaeus*, and *Bagualosaurus*) exhibit some dental traits associated with herbivory, suggesting a shift from the plesiomorphic carnivorous condition to an omnivorous diet (Bronzati et al., 2019; Müller and Garcia, 2019). In *Bagualosaurus*, this change in dietary habits was coupled with the acquisition of larger body size compared with other Carnian sauropodomorphs (Pretto et al., 2019). *Bagualosaurus* has a femoral length of ca. 21.5 cm (Pretto et al., 2019), indicating that it was about the same body size as *Thecodontosaurus*. This increase in body size could have promoted niche partitioning between *Bagualosaurus* and coeval sauropodomorphs (Bronzati et al., 2019; Müller and Garcia, 2019; Pretto et al., 2019). In this context, *Thecodontosaurus* is the basal-most sauropodomorph that exhibits dental traits related to herbivory, with straight, spear-like crowns and coarse, oblique serrations, as seen in more derived sauropodomorphs such as *Plateosaurus* (Prieto-Márquez and Norell, 2011) or *Unaysaurus* (Leal et al., 2004; McPhee et al., 2019). However, this typically herbivorous tooth morphology in *Plateosaurus* was accompanied by a cranial configuration that permitted facultative faunivorous habits (Button et al., 2016), a condition that seems to have been common among post-Carnian taxa (Barrett, 2000; Müller et al., 2018a). Therefore, *Thecodontosaurus* is one of the earliest sauropodomorphs that shifted to a predominantly herbivorous diet while probably maintaining occasional faunivorous habits.

Despite its larger body size compared with most Carnian sauropodomorphs, *Thecodontosaurus* shows a pelvic and hind limb morphology that indicates the retention of plesiomorphic locomotory traits. Its sigmoid femoral shape resembles that of more basal sauropodomorphs (Cabreira et al., 2016; Müller et al., 2018c; Langer et al., 2019; Pretto et al., 2019) and contrasts with the straighter femur of more derived post-Carnian taxa, a shape change that has been interpreted as indicating a gradual loss of cursoriality in the clade (Yates et al., 2010; Kubo and Kubo, 2012; Müller et al., 2018a). In addition, the ilium retains a plesiomorphic morphology, with an incompletely perforated acetabulum and an expanded supracetabular crest, indicating a lack of modifications in pelvic soft tissues associated with graviportalism and eventually quadrupedality that evolved in more derived sauropodomorphs (Tsai and Holliday, 2015; McPhee and Choiniere, 2016; Tsai et al., 2018). *Thecodontosaurus* is also the basal-most sauropodomorph to lack a trochanteric shelf, a dinosauriform apomorphy (Novas, 1996) that is absent in post-Carnian taxa (Müller et al., 2018a; McPhee et al., 2019) but is plesiomorphically retained by Carnian taxa, including *Bagualosaurus* (Cabreira et al., 2016; Müller et al., 2018c; Langer et al., 2019; Pretto et al., 2019), although the functional implications of this loss are not well understood apart from a possible reduction of M. iliofemoralis externus (Hutchinson, 2001b). In any case, pelvic and hind limb morphology in *Thecodontosaurus* indicates that it was an agile biped that retained plesiomorphic cursorial habits.

Thecodontosaurus was a key component of the Rhaetian fissure faunas of southwestern Britain. As a medium-sized, predominantly herbivorous biped, it was the main primary consumer of small island ecosystems (Whiteside et al., 2016) that were also inhabited by carnivorous coelophysoid dinosaurs (Whiteside and Marshall, 2008; Foffa et al., 2014; Keeble et al., 2018) that could have preyed on the former, as well as 'sphenosuchian' crocodylomorphs, diverse rhynchocephalians, and other lepidosaurs. These Late Triassic islands housed faunas that might have been similar to those of some modern reptile-dominated subtropical islands (Whiteside and Marshall, 2008). Additionally, the insular habitat of *Thecodontosaurus*, as well as its basal phylogenetic position, might explain the retention of a relatively small size compared with younger Norian taxa such as *Plateosaurus*. The stratigraphically late occurrence of such a phylogenetically plesiomorphic sauropodomorph as *Thecodontosaurus* might be explained by the fact it was an island-living dinosaur (Whiteside et al., 2016; Skinner et al., 2020); dwarfing and retention of primitive characters are commonly seen in island mammals and, for example, in the island dinosaurs of the Upper Cretaceous of Romania (Benton et al., 2010). Further work is required to better understand the complexity of these fissure faunas and the ecological relevance of *Thecodontosaurus* within them.

CONCLUSIONS

The early evolution and diversity of sauropodomorphs is increasingly understood owing to recent discoveries of Late Triassic species. The first sauropodomorph to be named, *Thecodontosaurus antiquus*, is one of the most basal members of the clade and an important taxon for the characterization of the morphological and functional modifications that occurred early in their evolution. The Tytherington sauropodomorph shares osteological features that support its assignment to *T. antiquus* and provides new information on previously unknown skeletal elements, notably within the skull. These findings cast doubt on the validity of *Pantydraco caducus* and *Asylosaurus yalensis*, and the former might represent a juvenile *T. antiquus* as originally proposed. *Thecodontosaurus*, together with findings from South America, documents an early shift toward a predominantly herbivorous diet in Sauropodomorpha, while maintaining a plesiomorphic posture, and was a key component of the Rhaetian fissure faunas of southwestern Britain.

ACKNOWLEDGMENTS

A.B. is funded by a NERC GW4+ Doctoral Training Partnership studentship from the Natural Environment Research Council (NE/L002434/1). We thank D. I. Whiteside for his information on the geology of the Tytherington fissure and helpful comments. We are grateful to P. Viegas and the volunteers of the Bristol Dinosaur Project who prepared the Tytherington material for several years at the University of Bristol under the supervision of M.J.B. We thank C. Hildebrandt, P. Russell, and A. Parker for their assistance during work on the University of Bristol collection, and D. Hutchinson for providing access to the Bristol City Museum and Art Gallery collection. We also thank R. T. Müller and B. W. McPhee for detailed reviews that greatly improved the quality of the manuscript. A.B. thanks A. Rodríguez de las Heras for his inspiration and encouragement to pursue a career in science and academia.

ORCID

Antonio Ballell http://orcid.org/0000-0001-8901-2398
Emily J. Rayfield http://orcid.org/0000-0002-2618-750X
Michael J. Benton http://orcid.org/0000-0002-4323-1824

LITERATURE CITED

Apaldetti, C., D. Pol, and A. Yates. 2013. The postcranial anatomy of *Coloradisaurus brevis* (Dinosauria: Sauropodomorpha) from the late Triassic of Argentina and its phylogenetic implications. Palaeontology 56:277–301.

Apaldetti, C., R. N. Martínez, O. A. Alcober, and D. Pol. 2011. A new basal sauropodomorph (Dinosauria: Saurischia) from Quebrada del Barro Formation (Marayes-El Carrizal Basin), northwestern Argentina. PLoS ONE 6:e26964.

Baron, M. G., D. B. Norman, and P. M. Barrett. 2017. A new hypothesis of dinosaur relationships and early dinosaur evolution. Nature 543:501–506.

Barrett, P. M. 2000. Prosauropod dinosaurs and iguanas: speculations on the diets of extinct reptiles; pp. 42–78 in H.-D. Sues (ed.), Evolution of Herbivory in Terrestrial Vertebrates: Perspectives from the Fossil Record. Cambridge University Press, Cambridge, U.K.

Barrett, P. M., K. E. J. Chapelle, C. K. Staunton, J. Botha, and J. N. Choiniere. 2019. Postcranial osteology of the neotype specimen of *Massospondylus carinatus* Owen, 1854 (Dinosauria: Sauropodomorpha) from the upper Elliot Formation of South Africa. Palaeontologia Africana 53:114–178.

Benton, M. J. 2012. Naming the Bristol dinosaur, *Thecodontosaurus*: politics and science in the 1830s. Proceedings of the Geologists' Association 123:766–778.

Benton, M. J., L. Juul, G. W. Storrs, and P. M. Galton. 2000. Anatomy and systematics of the prosauropod dinosaur *Thecodontosaurus antiquus* from the Upper Triassic of southwest England. Journal of Vertebrate Paleontology 20:77–108.

Benton, M. J., Z. Csiki, D. Grigorescu, R. Redelstorff, P. M. Sander, K. Stein, and D. B. Weishampel. 2010. Dinosaurs and the island rule: the dwarfed dinosaurs from Haţeg Island. Palaeogeography, Palaeoclimatology, Palaeoecology 293:438–454.

Bronzati, M., and O. W. M. Rauhut. 2018. Braincase redescription of *Efraasia minor* Huene, 1908 (Dinosauria: Sauropodomorpha) from the Late Triassic of Germany, with comments on the evolution of the sauropodomorph braincase. Zoological Journal of the Linnean Society 182:173–224.

Bronzati, M., R. T. Müller, and M. C. Langer. 2019. Skull remains of the dinosaur *Saturnalia tupiniquim* (Late Triassic, Brazil): with comments on the early evolution of sauropodomorph feeding behaviour. PLoS ONE 14:e0221387.

Bronzati, M., O. W. M. Rauhut, J. S. Bittencourt, and M. C. Langer. 2017. Endocast of the Late Triassic (Carnian) dinosaur *Saturnalia tupiniquim*: implications for the evolution of brain tissue in Sauropodomorpha. Scientific Reports 7:11931.

Brusatte, S. L., M. J. Benton, M. Ruta, and G. T. Lloyd. 2008a. Superiority, competition, and opportunism in the evolutionary radiation of dinosaurs. Science 321:1485–1488.

Brusatte, S. L., M. J. Benton, M. Ruta, and G. T. Lloyd. 2008b. The first 50 Myr of dinosaur evolution: macroevolutionary pattern and morphological disparity. Biology Letters 4:733–736.

Burch, S. H. 2014. Complete forelimb myology of the basal theropod dinosaur *Tawa hallae* based on a novel robust muscle reconstruction method. Journal of Anatomy 225:271–297.

Button, D. J., P. M. Barrett, and E. J. Rayfield. 2016. Comparative cranial myology and biomechanics of *Plateosaurus* and *Camarasaurus* and evolution of the sauropod feeding apparatus. Palaeontology 59:887–913.

Cabreira, S. F., C. L. Schultz, J. S. Bittencourt, M. B. Soares, D. C. Fortier, L. R. Silva, and M. C. Langer. 2011. New stem-sauropodomorph (Dinosauria, Saurischia) from the Triassic of Brazil. Naturwissenschaften 98:1035–1040.

Cabreira, S. F., A. W. A. Kellner, S. Dias-da-Silva, L. R. da Silva, M. Bronzati, J. C. A. Marsola, R. T. Müller, J. S. Bittencourt, B. J. Batista, T. Raugust, R. Carrilho, A. Brodt, and M. C. Langer. 2016. A unique Late Triassic dinosauromorph assemblage reveals dinosaur ancestral anatomy and diet. Current Biology 26:3090–3095.

Carrano, M. T., and J. R. Hutchinson. 2002. Pelvic and hindlimb musculature of *Tyrannosaurus rex* (Dinosauria: Theropoda). Journal of Morphology 253:207–228.

Chapelle, K. E., and J. N. Choiniere. 2018. A revised cranial description of *Massospondylus carinatus* Owen (Dinosauria: Sauropodomorpha) based on computed tomographic scans and a review of cranial characters for basal Sauropodomorpha. PeerJ 6:e4224.

Ezcurra, M. D. 2010. A new early dinosaur (Saurischia: Sauropodomorpha) from the Late Triassic of Argentina: a reassessment of dinosaur origin and phylogeny. Journal of Systematic Palaeontology 8:371–425.

Ezcurra, M. D., and C. Apaldetti. 2012. A robust sauropodomorph specimen from the Upper Triassic of Argentina and insights on the diversity of the Los Colorados Formation. Proceedings of the Geologists' Association 123:155–164.

Foffa, D., D. I. Whiteside, P. A. Viegas, and M. J. Benton. 2014. Vertebrates from the Late Triassic *Thecodontosaurus*-bearing rocks of Durdham Down, Clifton (Bristol, UK). Proceedings of the Geologists' Association 125:317–328.

Galton, P. M. 1973. On the anatomy and relationships of *Efraasia diagnostica* (Huene), n. gen., a prosauropod dinosaur (Reptilia: Saurischia) from the Upper Triassic of Germany. Paläontologische Zeitschrift 47:229–255.

Galton, P. M. 1985. Cranial anatomy of the prosauropod dinosaur *Sellosaurus gracilis* from the Middle Stubensandstein (Upper Triassic) of Nordwürttemberg, West Germany. Stuttgarter Beiträge zur Naturkunde, Series B 118:1–39.

Galton, P. M. 2007. Notes on the remains of archosaurian reptiles, mostly basal sauropodomorph dinosaurs, from the 1834 fissure fill (Rhaetian, Upper Triassic) at Clifton in Bristol, southwest England. Revue de Paléobiologie 26:505–591.

Galton, P. M., and D. Kermack. 2010. The anatomy of *Pantydraco caducus*, a very basal sauropodomorph dinosaur trom the Rhaetian (Upper Triassic) of South Wales, UK. Revue de Paléobiologie 29:341–404.

Galton, P. M., J. van Heerden, and A. M. Yates. 2005. Postcranial anatomy of referred specimens of the sauropodomorph dinosaur *Melanorosaurus* from the Upper Triassic of South Africa; pp. 1–37 in V. Tidwell and K. Carpenter (eds.), Thunder-Lizards: The Sauropodomorph Dinosaurs. Indiana University Press, Bloomington, Indiana.

Galton, P. M., A. M. Yates, and D. Kermack. 2007. *Pantydraco* n. gen. for *Thecodontosaurus caducus* Yates, 2003, a basal sauropodomorph dinosaur from the Upper Triassic or Lower Jurassic of South Wales, UK. Neues Jahrbuch für Geologie und Paläontologie, Abhandlungen 243:119–125.

Garcia, M. S., F. A. Pretto, S. Dias-da-Silva, and R. T. Müller. 2019. A dinosaur ilium from the Late Triassic of Brazil with comments on key-character supporting Saturnaliinae. Anais da Academia Brasileira de Ciencias 91:e20180614.

Holliday, C. M. 2009. New insights into dinosaur jaw muscle anatomy. Anatomical Record 292:1246–1265.

Huene, F. von. 1932. Die fossile Reptil-Ordnung Saurischia, ihre Entwicklung und Geschichte. Monographien zur Geologie und Paläontologie 4:1–361.

Hutchinson, J. R. 2001a. The evolution of pelvic osteology and soft tissues on the line to extant birds (Neornithes). Zoological Journal of the Linnean Society 131:123–168.

Hutchinson, J. R. 2001b. The evolution of femoral osteology and soft tissues on the line to extant birds (Neornithes). Zoological Journal of the Linnean Society 131:169–197.

Keeble, E., D. I. Whiteside, and M. J. Benton. 2018. The terrestrial fauna of the Late Triassic Pant-y-Ffynnon Quarry fissures, South Wales, UK and a new species of *Clevosaurus* (Lepidosauria: Rhynchocephalia). Proceedings of the Geologists' Association 129:99–119.

Kermack, D. 1984. New prosauropod material from South Wales. Zoological Journal of the Linnean Society 82:101–117.

Kubo, T., and M. O. Kubo. 2012. Associated evolution of bipedality and cursoriality among Triassic archosaurs: a phylogenetically controlled evaluation. Paleobiology 38:474–485.

Langer, M. C. 2003. The pelvic and hindlimb anatomy of the stem-sauropodomorph *Saturnalia tupiniquim* (Late Triassic, Brazil). Paleobios 23:1–40.

Langer, M. C., and J. Ferigolo. 2013. The Late Triassic dinosauromorph *Sacisaurus agudoensis* (Caturrita Formation; Rio Grande do Sul,

Brazil): anatomy and affinities. Geological Society, London, Special Publications 379:353–392.
Langer, M. C., M. A. G. Franca, and S. Gabriel. 2007. The pectoral girdle and forelimb anatomy of the stem-sauropodomorph *Saturnalia tupiniquim* (Upper Triassic, Brazil). Special Papers in Palaeontology 77:113–137.
Langer, M. C., F. Abdala, M. Richter, and M. J. Benton. 1999. A sauropodomorph dinosaur from the Upper Triassic (Carnian) of southern Brazil. Comptes Rendus de l'Académie des Sciences, Series IIA, Earth and Planetary Science 329:511–517.
Langer, M. C., B. W. McPhee, J. C. A. Marsola, L. R. da Silva, and S. F. Cabreira. 2019. Anatomy of the dinosaur *Pampadromaeus barberenai* (Saurischia–Sauropodomorpha) from the Late Triassic Santa Maria Formation of southern Brazil. PLoS ONE 14: e0212543.
Langer, M. C., M. D. Ezcurra, O. W. M. Rauhut, M. J. Benton, F. Knoll, B. W. McPhee, F. E. Novas, D. Pol, and S. L. Brusatte. 2017. Untangling the dinosaur family tree. Nature 551:e2.
Leal, L. A., S. A. K. Azevedo, A. W. A. Kellner, and A. A. S. Da Rosa. 2004. A new early dinosaur (Sauropodomorpha) from the Caturrita Formation (Late Triassic), Paraná Basin, Brazil. Zootaxa 690:1–24.
Marsh, A. D., and T. B. Rowe. 2018. Anatomy and systematics of the sauropodomorph *Sarahsaurus aurifontanalis* from the Early Jurassic Kayenta Formation. PLoS ONE 13:e0204007.
Marsola, J. C. A., G. S. Ferreira, M. C. Langer, D. J. Button, and R. J. Butler. 2019. Increases in sampling support the southern Gondwanan hypothesis for the origin of dinosaurs. Palaeontology 62:473–482.
Martínez, R. N. 2009. *Adeopapposaurus mognai*, gen. et sp. nov. (Dinosauria: Sauropodomorpha), with comments on adaptations of basal Sauropodomorpha. Journal of Vertebrate Paleontology 29:142–164.
Martínez, R. N., and O. A. Alcober. 2009. A basal sauropodomorph (Dinosauria: Saurischia) from the Ischigualasto Formation (Triassic, Carnian) and the early evolution of Sauropodomorpha. PLoS ONE 4:e4397.
Martínez, R. N., J. A. Haro, and C. Apaldetti. 2012. Braincase of *Panphagia protos* (Dinosauria, Sauropodomorpha). Journal of Vertebrate Paleontology 32(1, Supplement):70–82.
Martínez, R. N., P. C. Sereno, O. A. Alcober, C. E. Colombi, P. R. Renne, I. P. Montañez, and B. S. Currie. 2011. A basal dinosaur from the dawn of the dinosaur era in southwestern Pangaea. Science 331:206–210.
McPhee, B. W., and J. N. Choiniere. 2016. A hyper-robust sauropodomorph dinosaur ilium from the Upper Triassic–Lower Jurassic Elliot Formation of South Africa: implications for the functional diversity of basal Sauropodomorpha. Journal of African Earth Sciences 123:177–184.
McPhee, B. W., J. N. Choiniere, A. M. Yates, and P. A. Viglietti. 2015. A second species of *Eucnemesaurus* Van Hoepen, 1920 (Dinosauria, Sauropodomorpha): new information on the diversity and evolution of the sauropodomorph fauna of South Africa's lower Elliot Formation (latest Triassic). Journal of Vertebrate Paleontology. doi:10.1080/02724634.2015.980504.
McPhee, B. W., A. M. Yates, J. N. Choiniere, and F. Abdala. 2014. The complete anatomy and phylogenetic relationships of *Antetonitrus ingenipes* (Sauropodiformes, Dinosauria): implications for the origins of Sauropoda. Zoological Journal of the Linnean Society 171:151–205.
McPhee, B. W., J. S. Bittencourt, M. C. Langer, C. Apaldetti, and Á. A. S. Da Rosa. 2019. Reassessment of *Unaysaurus tolentinoi* (Dinosauria: Sauropodomorpha) from the Late Triassic (early Norian) of Brazil, with a consideration of the evidence for monophyly within non-sauropodan sauropodomorphs. Journal of Systematic Palaeontology 18:259–293.
Morris, J. 1843. A Catalogue of British Fossils. British Museum, London, 222 pp.
Müller, R. T. 2020. Craniomandibular osteology of *Macrocollum itaquii* (Dinosauria: Sauropodomorpha) from the Late Triassic of southern Brazil. Journal of Systematic Palaeontology 18:805–841.
Müller, R. T., and M. S. Garcia. 2019. Rise of an empire: analysing the high diversity of the earliest sauropodomorph dinosaurs through distinct hypotheses. Historical Biology. doi:10.1080/08912963.2019.1587754
Müller, R. T., M. C. Langer, and S. Dias-da-Silva 2018a. An exceptionally preserved association of complete dinosaur skeletons reveals the oldest long-necked sauropodomorphs. Biology Letters 14:20180633.
Müller, R. T., M. S. Garcia, Á. A. S. Da-Rosa, and S. Dias-da-Silva. 2018b. Under pressure: effect of sedimentary compression on the iliac morphology of early sauropodomorphs. Journal of South American Earth Sciences 88:345–351.
Müller, R. T., M. C. Langer, S. F. Cabreira, and S. Dias-da-Silva. 2015. The femoral anatomy of *Pampadromaeus barberenai* based on a new specimen from the Upper Triassic of Brazil. Historical Biology 28:656–665.
Müller, R. T., M. C. Langer, C. P. Pacheco, and S. Dias-da-Silva. 2019. The role of ontogeny on character polarization in early dinosaurs: a new specimen from the Late Triassic of southern Brazil and its implications. Historical Biology 31:794–805.
Müller, R. T., M. C. Langer, M. Bronzati, C. P. Pacheco, S. F. Cabreira, and S. Dias-da-Silva. 2018c. Early evolution of sauropodomorphs: anatomy and phylogenetic relationships of a remarkably well-preserved dinosaur from the Upper Triassic of southern Brazil. Zoological Journal of the Linnean Society 184:1187–1248.
Mussini, G., D. I. Whiteside, C. Hildebrandt, and M. J. Benton. 2019. Anatomy of a Late Triassic Bristol fissure: Tytherington fissure 2. Proceedings of the Geologists' Association. doi:10.1016/j.pgeola.2019.12.001.
Novas, F. E. 1994. New information on the systematics and postcranial skeleton of *Herrerasaurus ischigualastensis* (Theropoda: Herrerasauridae) from the Ischigualasto Formation (Upper Triassic) of Argentina. Journal of Vertebrate Paleontology 13:400–423.
Novas, F. E. 1996. Dinosaur monophyly. Journal of Vertebrate Paleontology 16:723–741.
Otero, A. 2018. Forelimb musculature and osteological correlates in Sauropodomorpha (Dinosauria, Saurischia). PLoS ONE 13: e0198988.
Otero, A., and D. Pol. 2013. Postcranial anatomy and phylogenetic relationships of *Mussaurus patagonicus* (Dinosauria, Sauropodomorpha). Journal of Vertebrate Paleontology 33:1138–1168.
Owen, R. 1842. Report on British fossil reptiles, Part II. Reports of the British Association for the Advancement of Science 11:60–204.
Pacheco, C., R. T. Müller, M. C. Langer, F. A. Pretto, L. Kerber, and S. D. da Silva. 2019. *Gnathovorax cabreirai*: a new early dinosaur and the origin and initial radiation of predatory dinosaurs. PeerJ 7: e7963.
Pol, D., and J. E. Powell. 2007. New information on *Lessemsaurus sauropoides* (Dinosauria: Sauropodomorpha) from the Upper Triassic of Argentina. Special Papers in Palaeontology 77:223–243.
Pol, D., A. Garrido, and I. A. Cerda. 2011. A new sauropodomorph dinosaur from the Early Jurassic of Patagonia and the origin and evolution of the sauropod type sacrum. PLoS ONE 6:e14572.
Porro, L. B., L. M. Witmer, and P. M. Barrett. 2015. Digital preparation and osteology of the skull of *Lesothosaurus diagnosticus* (Ornithischia: Dinosauria). PeerJ 3:e1494.
Pretto, F. A., M. C. Langer, and C. L. Schultz. 2019. A new dinosaur (Saurischia: Sauropodomorpha) from the Late Triassic of Brazil provides insights on the evolution of sauropodomorph body plan. Zoological Journal of the Linnean Society 185:388–416.
Prieto-Márquez, A., and M. A. Norell. 2011. Redescription of a nearly complete skull of *Plateosaurus* (Dinosauria: Sauropodomorpha) from the Late Triassic of Trossingen (Germany). American Museum Novitates 3727:1–58.
Riley, H., and S. Stutchbury. 1836. A description of various fossil remains of three distinct saurian animals discovered in the autumn of 1834, in the Magnesian Conglomerate on Durdham Down, near Bristol. Proceedings of the Geological Society of London 2:397–399.
Riley, H., and S. Stutchbury. 1840. A description of various fossil remains of three distinct saurian animals, recently discovered in the Magnesian Conglomerate near Bristol. Transactions of the Geological Society of London, Series 2 5:349–357.
Seeley, H. G. 1887. On the classification of the fossil animals commonly named Dinosauria. Proceedings of the Royal Society of London 43:165–171.
Sereno, P. C. 1994. The pectoral girdle and forelimb of the basal theropod *Herrerasaurus ischigualastensis*. Journal of Vertebrate Paleontology 13:425–450.

Sereno, P. C. 2007. Basal Sauropodomorpha: historical and recent phylogenetic hypotheses, with comments on *Ammosaurus major* (Marsh, 1889). Special Papers in Palaeontology 77:261–289.

Sereno, P. C., R. N. Martínez, and O. A. Alcober. 2013. Osteology of *Eoraptor lunensis* (Dinosauria, Sauropodomorpha). Journal of Vertebrate Paleontology 32(1, Supplement):83–179.

Sertich, J. J., and M. A. Loewen. 2010. A new basal sauropodomorph dinosaur from the Lower Jurassic Navajo Sandstone of southern Utah. PLoS ONE 5:e9789.

Skinner, M., M. J. Benton, and D. I. Whiteside. 2020. Late Triassic island dwarfs? Terrestrial tetrapods of the Ruthin fissure (South Wales, UK) including a new genus of procolophonid. Proceedings of the Geologists' Association. doi:10.1016/j.pgeola.2020.04.005.

Tsai, H. P., and C. M. Holliday. 2015. Articular soft tissue anatomy of the archosaur hip joint: structural homology and functional implications. Journal of Morphology 276:601–630.

Tsai, H. P., K. M. Middleton, J. R. Hutchinson, and C. M. Holliday. 2018. Hip joint articular soft tissues on non-dinosaurian Dinosauromorpha and early Dinosauria: evolutionary and biomechanical implications for Saurischia. Journal of Vertebrate Paleontology. doi:10.1080/02724634.2017.1427593.

Wedel, M. 2003. The evolution of vertebral pneumaticity in sauropod dinosaurs. Journal of Vertebrate Paleontology 23:344–357.

Wedel, M. 2007. What pneumaticity tells us about 'prosauropods', and vice versa. Special Papers in Palaeontology 77:207–222.

Whiteside, D. I. 1983. A fissure fauna from Avon. Ph.D. dissertation, University of Bristol, Bristol, U.K., 216 pp.

Whiteside, D. I., and J. E. A. Marshall. 2008. The age, fauna and palaeoenvironment of the Late Triassic fissure deposits of Tytherington, South Gloucestershire, UK. Geological Magazine 145:105–147.

Whiteside, D. I., C. J. Duffin, P. G. Gill, J. E. A. Marshall, and M. J. Benton. 2016. The Late Triassic and Early Jurassic fissure faunas from Bristol and South Wales: stratigraphy and setting. Palaeontologia Polonica 67:257–287.

Wilson, J. A. 2002. Sauropod dinosaur phylogeny: critique and cladistic analysis. Zoological Journal of the Linnean Society 136:215–275.

Wilson, J. A., M. D. D'Emic, T. Ikejiri, E. M. Moacdieh, and J. A. Whitlock. 2011. A nomenclature for vertebral fossae in sauropods and other saurischian dinosaurs. PLoS ONE 6:e17114.

Yates, A. M. 2003a. A new species of the primitive dinosaur *Thecodontosaurus* (Saurischia: Sauropodomorpha) and its implications for the systematics of early dinosaurs. Journal of Systematic Palaeontology 1:1–42.

Yates, A. M. 2003b. The species taxonomy of the sauropodomorph dinosaurs from the Löwenstein Formation (Norian, Late Triassic) of Germany. Palaeontology 46:317–337.

Yates, A. M. 2004. *Anchisaurus polyzelus* (Hitchcock): the smallest known sauropod dinosaur and the evolution of gigantism among sauropodomorph dinosaurs. Postilla 230:1–58.

Yates, A. M. 2007. The first complete skull of the Triassic dinosaur *Melanorosaurus* Haughton (Sauropodomorpha: Anchisauria). Special Papers in Palaeontology 77:9–55.

Yates, A. M., and J. W. Kitching. 2003. The earliest known sauropod dinosaur and the first steps towards sauropod locomotion. Proceedings of the Royal Society B: Biological Sciences 270:1753–1758.

Yates, A. M., M. F. Bonnan, and J. Neveling. 2011. A new basal sauropodomorph dinosaur from the Early Jurassic of South Africa. Journal of Vertebrate Paleontology 31:610–625.

Yates, A. M., M. J. Wedel, and M. F. Bonnan. 2012. The early evolution of postcranial skeletal pneumaticity in sauropodomorph dinosaurs. Acta Palaeontologica Polonica 57:85–100.

Yates, A. M., M. F. Bonnan, J. Neveling, A. Chinsamy, and M. G. Blackbeard. 2010. A new transitional sauropodomorph dinosaur from the Early Jurassic of South Africa and the evolution of sauropod feeding and quadrupedalism. Proceedings of the Royal Society B: Biological Sciences 277:787–794.

Submitted November 21, 2019; revisions received February 26, 2020; accepted March 30, 2020.
Handling editor: Lindsay Zanno.